Environmental Research 275 (2025) 121446

Contents lists available at ScienceDirect

Environmental Research

journal homepage: www.elsevier.com/locate/envres

Can biochar fillers advance the properties of composites? Early-stage characterization and life cycle assessment of novel polyamide/biochar biocomposites

Hossein Baniasadi [a,**,1], Laura Äkräs [a,1], Zoe Paganelli [a], Nele Dammann [a], Roozbeh Abidnejad [b], Sami Lipponen [a], Frans Silvenius [c], Marjatta Vahvaselkä [d], Hannu Ilvesniemi [d], Jukka Seppälä [a], Jukka Niskanen [a,*]

[a] Polymer Synthesis Technology, School of Chemical Engineering, Aalto University, Kemistintie 1, 02150, Espoo, Finland
[b] Department of Bioproducts and Biosystems, School of Chemical Engineering, Aalto University, Aalto, FI-00076, Finland
[c] Bioeconomy and Environment, Natural Resources Institute Finland, Latokartanonkaari 9, 00790, Helsinki, Finland
[d] Production Systems, Natural Resources Institute Finland, Latokartanonkaari 9, 00790, Helsinki, Finland

ARTICLE INFO

Keywords:
Polyamide 1010
Biochar
Biocomposite
Characterization
Life cycle assessment

ABSTRACT

In response to growing environmental concerns, this study explores the potential of polyamide 1010 (PA1010) and biochar biocomposites as a sustainable solution in polymer engineering. The research addresses the gap in reinforcing biocomposites with biochar, demonstrating enhanced physical properties and reduced environmental impact. Scanning electron microscopy (SEM) revealed excellent biochar dispersion and strong adhesion with the PA1010 matrix. Mechanical testing showed significant improvements, including a 44 % increase in tensile strength and a 110 % increase in tensile modulus. Thermal stability also improved, increasing decomposition temperature from 460 °C to 474 °C. Additionally, dynamic mechanical analysis (DMA) and rheology tests confirmed increased stiffness and flow resistance. Life cycle assessment (LCA) highlighted a 65 % reduction in carbon footprint, indicating the environmental benefits of these biocomposites. These findings position PA1010/biochar biocomposites as promising materials for sustainable applications in engineering, particularly in industries seeking to reduce environmental impact while enhancing performance.

1. Introduction

Polyamides (PAs) are a versatile class of polymers known for their wide-ranging properties and applications. Their long-chain molecular structure, characterized by amide bonds, facilitates hydrogen bonding between polymer chains, enhancing crystallization. This unique molecular arrangement imparts high tensile strength, toughness, and flexibility to PAs. Additionally, PAs exhibit excellent chemical resistance and low friction coefficients, making them suitable for demanding applications (Baniasadi et al., 2023b; Fu et al., 2020; Li et al., 2023; Madani et al., 2024). However, the widespread use of petroleum-based PAs presents significant environmental challenges. These include fossil resource depletion, the accumulation of non-biodegradable PA waste, and the release of harmful chemicals and microplastics during degradation. Additionally, since PA production relies on fossil fuels, it contributes to greenhouse gas (GHG) emissions, exacerbating climate change (Alijagic et al., 2024; Baniasadi et al., 2023c; Costamagna et al., 2023).

Bio-based PAs have emerged as a promising alternative. Unlike their fossil-derived counterparts, bio-based PAs are produced from renewable biomass sources, such as castor oil, which is rich in ricinoleic acid—a key building block for bio-based PAs. These materials offer a more sustainable solution, reducing dependence on finite fossil fuels and mitigating GHG emissions (Mi et al., 2024; Zierdt et al., 2015). A notable example is PA1010, synthesized through polycondensation of castor oil derivatives: sebacic acid and 1,10-diaminodecane. PA1010 exhibits properties comparable to traditional PAs, including high strength, chemical resistance, and thermal stability, making it a viable option for

* Corresponding author.
** Corresponding author.
E-mail addresses: hossein.baniasadi@aalto.fi (H. Baniasadi), jukka.niskanen@aalto.fi (J. Niskanen).
[1] HB, and LÄ contributed equally to this work.

https://doi.org/10.1016/j.envres.2025.121446
Received 11 December 2024; Received in revised form 3 March 2025; Accepted 19 March 2025
Available online 20 March 2025

automotive, electronics, and consumer goods applications (Alijagic et al., 2024; Lu et al., 2017; Quiles-Carrillo et al., 2019).

Another strategy for reducing the environmental impact of plastics involves the integration of biochar. Biochar is a carbon-rich material resulting from the pyrolysis of biomass or organic waste such as agricultural residues, wood chips, and municipal solid. The production of biochar leads to carbon sequestration by trapping CO_2 within the material matrix, resulting in environmental benefits (Arjona-Jaime et al., 2024; Francis et al., 2023; Roy et al., 2025). Hence, Incorporating biochar into biocomposites can lower CO_2 emissions, enhance mechanical properties, and promote circular economy principles by utilizing waste materials (Baniasadi et al., 2024; Kane et al., 2022; Phiri et al., 2023). However, a comprehensive life cycle assessment (LCA) is required to quantify these environmental benefits accurately.

While the environmental impact of biochar as a standalone material has been extensively studied (Azzi et al., 2021; Brassard et al., 2021; Matuštík et al., 2020; Peters et al., 2015), LCAs focusing on biochar-filled composites remain scarce. Only a handful of studies exist, including a comparative, cradle-to-grave LCA of talc- and biochar-reinforced polypropylene (PP) with a filler content of 30 wt% (Tadele et al., 2020), a cradle-to-grave LCA of laboratory-scale biochar/miscanthus fiber- and talc/colorant-reinforced PP (Roy et al., 2020), followed by a cradle-to-gate LCA of recycled high-density polyethylene (HDPE), virgin HDPE, polylactic acid (PLA), and polyhydroxybutyrate, reinforced with up to 40 wt% of biochar (Kane et al., 2022). Furthermore, these papers were accompanied by a laboratory-scale cradle-to-gate LCA of a composite adsorbent made of pomace leaves-based biochar and plastic waste (Osman et al., 2022), as well as a review of the prospects of composites in the automotive industry, also including the use of biochar as a filler and the environmental impacts of these composites (Roy et al., 2019). Surprisingly, only one study quantified the environmental impact of bio-based polyamide 12 (PA12) filled with biochar—derived either from cultivated biomass or waste streams (Baniasadi et al., 2024). Most LCA studies have focused on polyolefin matrices (Kane et al., 2022; Roy et al., 2020; Tadele et al., 2020), with only one incorporating a bio-based PA. Additionally, biochar sources have primarily included Miscanthus grass (Roy et al., 2020; Tadele et al., 2020), forestry residues (Kane et al., 2022), pomace leaves (Osman et al., 2022), natural fibers (Roy et al., 2019), and wood chips (Baniasadi et al., 2024).

Notably, no LCA studies have specifically assessed the environmental impact of bio-based PA1010 composites, particularly those incorporating wood chip-derived biochar. This highlights a critical gap in the literature and underscores the need for further research on PA/biochar (bio)composites. Considering previous studies have primarily explored polyolefin-based biochar composites, our research focuses on a renewable, bio-based PA1010 matrix reinforced with wood chip-derived biochar. This innovative material combination enhances sustainability while also providing valuable insights into the performance-to-environmental impact trade-offs. By conducting a comprehensive cradle-to-gate LCA, our study bridges a significant knowledge gap, offering a more sustainable and high-performance alternative for future biocomposites.

2. Experiments and methodology

2.1. Materials

PA1010 plastic granules were procured from Arkema, France, while the wood chips – sourced from pine – were purchased from a local supplier in Finland.

2.2. Preparation of biochar

The wood chips underwent pyrolysis at 550 °C under a nitrogen atmosphere using a furnace (Nabertherm tube furnace model RHTH 80–300/16). The heating rate was maintained at 5 °C/min, and the sample was isothermally held at 550 °C for 2 h. Subsequently, the resulting pyrolyzed sample, termed biochar, was milled using a planetary ball mill (Fritsch Pulverisette 6 Ball Mill) and sieved through a 70 μm sieve prior to compounding with the PA1010 granules.

2.3. Melt compounding and injection molding

Various concentrations of biochar were melt blended with the PA1010 granules by employing a counter-rotating twin extruder (Labtech Extruder model LTE 20–44). The extruder featured five heating zones with temperature profiles set at 220 °C, 230 °C, 240 °C, 240 °C, and 240 °C, respectively, while the screw speed was fixed at 50 rpm. The estimated shear rate within the extruder ranged between 100 and 300 s^{-1}, depending on biochar concentration. The average residence time in the extruder was approximately 2–3 min, ensuring adequate dispersion of biochar without significant thermal degradation. Subsequently, the resulting compounds were pelletized into granules. The mass ratios of the PA1010 granules and biochar in the biocomposites were varied as 100/0, 90/10, 70/30, and 50/50, with the corresponding samples designated as PA1010, PA1010-BC10, PA1010-BC30, and PA1010-BC50, respectively. The digital images of the injection-molded PA1010 and PA1010-BC50 are shown in Fig. S1. The selected biochar concentrations (10 %, 30 %, and 50 %) were chosen to systematically investigate the structure-property correlations, representing low, medium, and high filler loadings. Noteworthily, it was not feasible to test higher concentrations of biochar due to the material's hardness, which posed constraints on the extrusion process. Specifically, attempts to incorporate biochar beyond 50 % were unsuccessful, as the twin-screw extruder immediately reached its maximum torque, causing the motors to stop automatically. This limitation prevented the homogeneous mixing of higher biochar contents, further reinforcing the chosen concentration range.

The composite granules were then fed into an injection molding machine (Engel ES 200/40) to fabricate specimens (conforming to ISO 527, specimen type 1A) for tensile and impact assessments. All the heating zones were set at 230 °C with a dosing speed of 50 % and a counter pressure of 7 bar. An injection speed of 75 mm/s was utilized during the injection phase with a mold temperature of 40 °C, which was followed by an after-pressure phase of 45 bar for 20 s.

2.4. Life cycle assessment

2.4.1. Goal and scope definition

The primary objective of the present cradle-to-gate LCA was to comprehensively evaluate the diverse environmental impacts regarding bio-based materials, as well as to pinpoint the critical areas of concern associated with the newly developed PA1010/biochar biocomposites by following the methodological guidelines outlined in ISO 14040:2006 and 14044:2006 (Baniasadi et al., 2025a) standards. This acquired information could further optimize the current laboratory-scale processes and possibly be used as *ex-ante* LCA. The utilization of *ex-ante* LCA would help to gain a more accurate understanding of the PA1010/biochar biocomposites on the industrial scale (Äkräs et al., 2024; Piccinno et al., 2015) when the utilized technologies have become mature (Baniasadi et al., 2025b; Cucurachi et al., 2018).

The functional unit for the LCA was defined as a mass-based 1 kg of biocomposite granules. The study also considered the first half of the life cycle of biocomposites, from the cultivation of biomass to its further processing and conversion into industrially produced raw materials: castor beans, PA1010 granules, and wood chips. The transportation of these raw materials and the laboratory-scale manufacturing of PA1010/biochar biocomposite granules were also included within the system boundaries (Fig. 1). Nonetheless, the use and End-of-Life (EoL) phases were excluded from the system boundaries since the biocomposites are still at their early development stage, can still be used for further

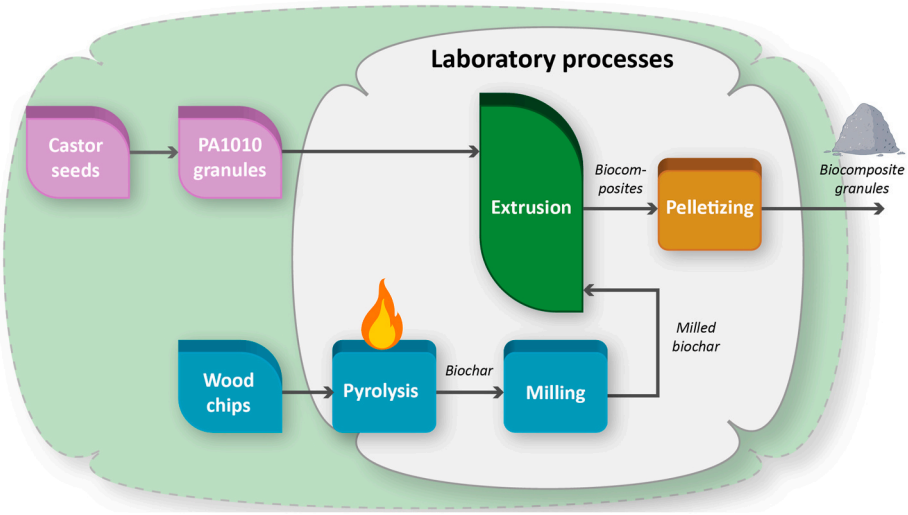

Fig. 1. A simplified scheme representing the cradle-to-gate system boundaries used for the LCA. The small colored shapes represent the different unit processes, while the arrows stand for the main mass flows between these processes, and – finally – the dashed line delimits the whole system under analysis. Transportation of raw materials is not depicted in this scheme.

production as input materials, and have not yet solidly defined applications or experimentally explored EoL pathways. Additionally, combining industrial-scale EoL pathways with laboratory-scale biocomposites could have derived misleading results and conclusions. The selected cradle-to-gate approach is viable, and it has previously been employed by Piccinno et al. (2015) and Röder et al. (2022). Furthermore, injection molding was omitted from the system boundaries since it was used as a characterization method instead of a synthesis method. Concurrently, the selection of laboratory scale for the present LCA was reasoned by the objective of the study, namely the early-stage development of the biocomposites and the complexity of a theoretical scaling up in the absence of suitable frameworks.

The primary geographical focus of the study was Finland. Nevertheless, India and France were considered for the cultivation of castor beans and the production of PA1010 granules, respectively. The target audience for this study was carefully chosen to include scholars, policymakers, and industrial stakeholders involved in the exploration and implementation of innovative and potentially more sustainable material alternatives. Lastly, the comparison of the acquired LCIA results to the ones of commercial fossil-based plastics and the laboratory-scale composites, available in the reports of PlasticsEurope and literature (Piccinno et al., 2016), was omitted from the study due to the different methodological decisions between the studies and the limited number of comparable impact categories. However, the LCIA results of the PA1010/biochar biocomposites were directly compared with the selected commercial and sustainable composites, along with a set of polyamide-based composites at their early stage of development.

2.4.2. Life cycle inventory (LCI)

The LCI utilized in the present LCA draws upon primary, secondary, and tertiary data sources. Specifically, LCI data for the laboratory-scale processes of pyrolysis, milling, extrusion, and pelletizing were gathered during the experimental procedures and supplemented by literature values, calculations, and/or assumptions (Equations S1-S3). Additionally, these data were enriched with auxiliary process datasets available in Sphera Solutions GmbH's Managed LCA Content (MLC) 2023.2 databases (Sphera, 2024a) within the LCA for Experts (LCA FE) software (Sphera, 2024b). Similarly, the LCI data about the acquisition and processing of castor beans and PA1010 granules were purchased from Sphera Solutions GmbH, whilst the information required to model the production of wood chips was extracted from the Sphera Solution GmbH's MLC 2023.2 databases. Conversely, the transportation of raw materials to Aalto University, where the study was conducted, relied mainly on assumptions derived from relevant websites, such as Google Maps, Fluent Cargo, and SeaRates, along with the auxiliary process datasets obtained from the Sphera's MLC 2023.2 databases. A comprehensive compilation of all the LCI data and auxiliary process datasets utilized is presented in Tables S1–S7 and Tables S8-S11, respectively. It is worth noting that the purchased datasets have been excluded from these tables due to their commercial origin and in adherence to the guidelines established by Sphera Solutions GmbH.

2.4.3. Data and modeling assumptions

Several assumptions were made when constructing the LCI and modeling the system boundaries. Initially, the power of the pyrolysis furnace and extruder was estimated based on the findings reported by Hopkinson et al. (2011), incorporating a reduction factor of 33 % derived from the oven (a proxy equipment for the pyrolysis chamber and extruder). By utilizing the oven as the proxy equipment, a more realistic assessment of the electricity consumption for the pyrolysis chamber and extruder was obtained. Furthermore, the resulting electricity values from the pyrolysis and extrusion processes were cross-referenced with literature data, yielding a consistent outcome of the same order of magnitude, i.e., 2 kWh/kg for both processes (Njobet, 2012; Tadele et al., 2020). Similarly, the electricity consumption of the pelletizer/milling equipment was calculated based on the equipment's power and usage time (Ang et al., 2020). Nonetheless, estimations were made for power and usage time values in instances of missing data or when there was a need to ascertain actual equipment usage.

A literature value for cooling water of an industrial extruder was used as an estimate for one of the laboratory-scale extruders of the present LCA (Maga et al., 2019). The utilized value is comparable with the value of solvents in a previous laboratory-scale LCA study (Iliescu, 2023). Negligible amounts of waste or substance residues generated during the laboratory experiments, along with the potential cleaning water and typical co-products of biochar (specifically, bio-oil and syngas), were excluded from the LCI. The latter was due to the collection of syngas with the nitrogen flow and the absence of bio-oil formation during the pyrolysis process. Furthermore, the composition of carbon, nitrogen, and oxygen in biochar needed to be partly approximated as a base for further calculations, while the German process for PA1010 granules was utilized in LCA FE due to the lack of a French version. Lastly, the transport distances and points of arrival and departure, although selected based on available information and logical reasoning,

were regarded as assumptions rather than incontrovertible data.

2.4.4. Sensitivity analysis

Sensitivity analysis was an essential aspect of the present study, assessing the uncertainty associated with the data and modeling decisions. Notably, the analysis identified electricity usage as the primary contributor to the environmental burdens across all the laboratory-scale processes. Consequently, a sensitivity analysis scenario (denoted as SA1) was implemented, utilizing global green electricity, to provide insight into the potential mitigation strategies and their impact on the final results. Nonetheless, the purchased datasets from Sphera or the process for wood chips could not be modified upon modeling, which is why green electricity was only used for the laboratory-scale processes in SA1.

2.4.5. Life cycle impact assessment (LCIA)

Sphera's LCA FE software served as the platform for conducting the LCA presented in this paper. The LCIA method employed was EF 3.1, which enabled the quantification of the diverse environmental impacts associated with the PA1010/biochar biocomposite granules. Within LCA FE, the selected impact categories included carbon footprint, acidification, eutrophication (terrestrial, freshwater, and marine), and land use. Furthermore, the sequestered CO_2 in biochar was calculated by using Equation (1), which was formulated based on the work of Kane et al. (2022). A more detailed explanation of calculating the amount of sequestered CO_2 in biochar is available in Equations S4-S7 and Table S12.

$$CO_2(biochar) = \frac{M(C_{biochar})}{M(biochar)}\ x\ m(biochar_{biocomposite})\ x\ \frac{1\ mol\ C}{12\ kg\ C}\ x\ \frac{1\ mol\ CO_2}{1\ mol\ C}\ x\ \frac{44\ kg\ CO_2}{1\ mol\ CO_2} \quad (1)$$

Here, $M(C_{biochar})$ and $M(biochar)$ denote the molecular weight of carbon in biochar and biochar itself, respectively, in grams per mole (g/mol), while $m(biochar_{biocomposite})$ represents the carbon content of biochar in kg for 1 kg of biocomposite granules.

2.5. Characterization methods

2.5.1. Fourier transform infrared spectroscopy (FTIR)

The functional groups of the biochar, PA1010, and their corresponding biocomposites were analyzed by using FTIR with an ATR device, performed on a PerkinElmer FTIR. The wavenumber range was set between 4000 cm^{-1} and 500 cm^{-1}, with a resolution of 4 cm^{-1} and 16 scans per measurement. Before the measurements, the background was also scanned using the same parameters. The integral areas of the peaks at 3299 cm^{-1} (A_1) and 1633 cm^{-1} (A_2) were used to calculate the hydrogen bonding index (*HBI*) according to Equation (2) (Baniasadi et al., 2023a).

$$HBI = \frac{A_1}{A_2} \quad (2)$$

2.5.2. Scanning electron microscopy (SEM)

The morphology of the biochar, PA1010 granules, and biocomposites was examined by using SEM images obtained with the Zeiss Sigma VP device. All samples underwent a thin coating (~4 nm) of gold-palladium prior to imaging at an operating voltage of 2 kV. Additionally, elemental composition analysis was performed using X-ray spectroscopy (EDX) to complement the SEM observations.

2.5.3. Characterization of crystallinity

The crystallinity of the biocomposites was determined through DSC conducted on the TA Instruments Discovery DSC model 250 Auto. Approximately 5 mg of each sample was sealed within a Tzero aluminum pan and subjected to two heating and cooling cycles under a nitrogen atmosphere. With a fixed heating and cooling rate of 10 °C/min, the temperature range spanned from 0 °C to 250 °C. The second heating and cooling cycles were utilized to extract the key parameters, such as melting (T_m) and crystallization (T_c) temperatures, as well as melting (ΔH_m) and crystallization (ΔH_c) enthalpies. The melting enthalpy (ΔH_m) was subsequently employed to calculate crystallinity (χ_c) by using Equation (3), where ΔH_m^0 represents the melting crystallization of 100 % crystalline PA1010 (i.e., 244 J/g (Hernández-García et al., 2023)), and x denotes the fraction of biochar in the sample.

$$\chi_c(\%) = \frac{\Delta H_m}{\Delta H_m^0(1-x)} \times 100 \quad (3)$$

The crystallinity of the samples was additionally examined by using X-ray diffraction (XRD) on the PANalytical X'Pert MPD Alpha 1 system from the Netherlands. Data were collected over an angular range of 5–40° (2θ) with an operating voltage of 45 kV and a current of 40 mA, employing X-ray radiation at a wavelength of 1.54 Å.

2.5.4. Thermogravimetric analysis (TGA)

The thermal decomposition behavior of the developed biocomposites was investigated under a nitrogen atmosphere by using TGA performed on a TA Instruments model TGA 5500. The samples were initially equilibrated at 30 °C before being heated to 800 °C at a rate of 10 °C/min. Thermal decomposition temperatures, including 5 % and 10 %, and maximum decomposition temperatures ($T_{5\ \%}$, $T_{10\ \%}$, T_{max}), as well as residue at 800 °C, were extracted and analyzed from the TGA and derivative thermogravimetric (DTG) curves.

2.5.5. Evaluation of mechanical properties

The tensile properties of the biocomposites were evaluated through tensile testing performed on a Universal Tester Instron device model 4204 by following the ASTM D638 standards. Conditioning for 48 h at 23 °C and 55 % relative humidity preceded the measurements. Tensile modulus, tensile strength, and tensile strain data were extracted and analyzed from typical stress-strain curves. Additionally, a three-point bending test was performed on a specimen measuring 125 mm × 13 mm × 3 mm following the ASTM D790 standards to ascertain its flexural properties. Moreover, the impact strength was measured based on ASTM D256 by using the Izod impact strength test with a 1 J hammer after machining a V-shape notch with a depth of 1.2 mm on the sample. Multiple measurements (at least three replicates) were conducted for each sample to ensure statistical relevance. The statistical analysis of the mechanical properties, including ANOVA, was performed with a p-value less than 0.05, indicating the statistical significance of the results.

2.5.6. Dynamic mechanical analysis

The dynamic mechanical properties were also assessed by using a TA Instruments device model Q800 under a multi-frequency-strain procedure mode. Strip-shaped biocomposite samples were clamped in the device, while preload, strain, and frequency were set at 1 N, 1 %, and 1 Hz, respectively. The temperature ramped from 0 °C to 200 °C at a heating rate of 5 °C/min, and trends of storage modulus (E') and tan δ versus temperature were analyzed.

2.5.7. Characterization of rheology

The rheology characteristics of the biocomposites were studied at 230 °C by using an Anton Paar Physica rheometer model MCR 301. A strain sweep test was first conducted across the range of 0.01 %–100 % at a constant angular frequency of 10 rad/s to identify the linear viscoelastic region. Subsequently, a frequency sweep test was carried out at a fixed shear strain rate of 1 %, with the angular frequency ramped logarithmically from 0.01 rad/s to 628 rad/s. Complex viscosity ($|\eta^*|$), storage modulus (G′), and loss modulus (G″) behaviors were also investigated based on the results obtained from the frequency sweep test.

3. Results and discussion

3.1. Characterization of biocomposites

3.1.1. FTIR spectroscopic analysis

FTIR spectroscopy was employed to study the functional groups and structural characteristics of biochar, PA1010, and the corresponding biocomposites. The results are provided in Fig. 2a. The FTIR spectrum of PA1010 prominently featured several key peaks confirming the presence of polyamide functionality (Baniasadi et al., 2021a; Baniasadi and Seppälä, 2021): a broad peak around 3300 cm^{-1}, indicating N-H stretching vibrations associated with the amide groups; a strong peak at approximately 1640 cm^{-1}, corresponding to C=O stretching vibrations in the amide linkages; a peak near 1540 cm^{-1}, attributed to N-H bending and C-N stretching vibrations; and a peak around 1230 cm^{-1}, related to C-N stretching within the polyamide backbone. In contrast, the FTIR spectrum of biochar showed a reduction or absence of characteristic peaks of the original wood, reflecting the substantial volatilization of organic matter during the carbonization process. For the PA1010/biochar biocomposites, the FTIR spectrum generally retained the characteristic peaks of PA1010 but exhibited variations in intensity and slight shifts. These changes are attributed to the interaction between PA1010 and biochar, which may alter the spectral features.

The HBI values, calculated using Equation (2), are summarized in Fig. 2b. The incorporation of biochar initially increased the HBI, suggesting enhanced hydrogen bonding interactions and potentially improved material cohesion or biocomposite properties. However, the HBI slightly decreased in the biocomposites with the highest biochar content, such as PA1010-BC50. This reduction indicates a decrease in hydrogen bonding strength, which may be due to the disruption of the polyamide matrix by the high concentration of biochar particles. Such interference could disrupt the hydrogen bonding network and diminish overall bonding efficiency.

3.1.2. Microstructure of biocomposites

It is widely recognized that filler dispersion and filler-polymer interfacial interaction are critical determinants influencing the properties of the resulting composites (Alghyamah et al., 2021). Consequently, SEM images were employed to examine the degree of biochar dispersion and the interface quality between biochar and the PA1010 matrix, aiming to assess factors like adhesion and interlocking, which directly influence load transfer and mechanical performance. The SEM micrographs of biochar, pure PA1010, and the developed biocomposites are provided in Fig. 3. Biochar particles (Fig. 3a) exhibited a random shape morphology, with most particles ranging from thin sheets to irregularly shaped chunks, aligning with the reported morphologies for pyrolyzed softwood prepared with similar carbonization processes (George et al., 2019; Mohammed et al., 2022). As anticipated, the particles were less than 70 μm, consistent with the size of the sieve used for sieving the milled biochar particles. Upon magnification (Fig. 3b), surface micro-sized pores were apparent on the carbon surface, likely formed during the carbonization process. These pores enhanced the biochar's surface area, facilitating increased interaction and improving adhesion between the biochar and the polymer matrix. This enhancement contributed to increased mechanical strength and durability of the biocomposites.

Consequently, the morphology of the resulting biocomposites was inspected by SEM images to assess the interaction quality between the PA1010 matrix and biochar particles and to monitor the filler dispersion levels in the matrix. Pure PA1010 (Fig. 3c) exhibited a relatively smooth and flat fracture surface with limited plastic deformation. In contrast, biocomposite samples containing biochar (Fig. 3d–f) displayed notably different fracture surface morphology. Specifically, regions with increased roughness and irregularities were observed, particularly where biochar particles were covered by the polymer matrix. Notably, upon increasing biochar content, the fillers were more and more uniformly dispersed throughout the matrix without any indications of particle agglomeration, pull-out, debonding, crack formation, or phase separation. These observations signify excellent compatibility and interface adhesion between the components, as well as appropriate bonding between the PA chains and biochar particles. This phenomenon can be attributed to the large surface area and porous structure of the prepared biochar, a characteristic also supported by the findings of other research groups (Alghyamah et al., 2021; Das et al., 2021; Sobhan et al., 2021). Remarkably, no compatibilizer was employed to enhance filler-polymer interfacial bonding, affirming that the observed trend of enhanced interface quality is solely due to the inherent characteristics of biochar. The failure mode appeared to be ductile, with good adhesion and dispersion of biochar particles, contributing to improved mechanical performance.

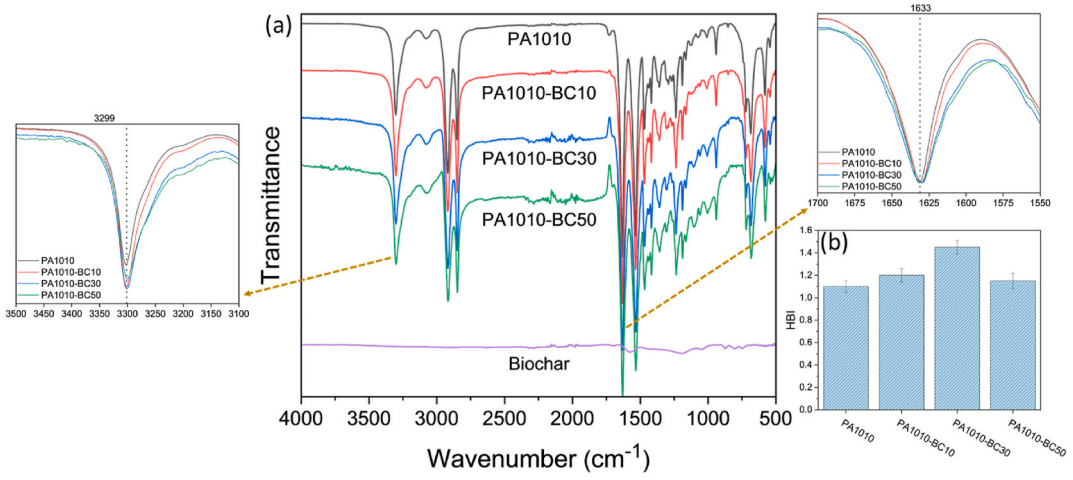

Fig. 2. (a) FTIR spectra and (b) HBI analysis of PA1010 and its corresponding biocomposites.

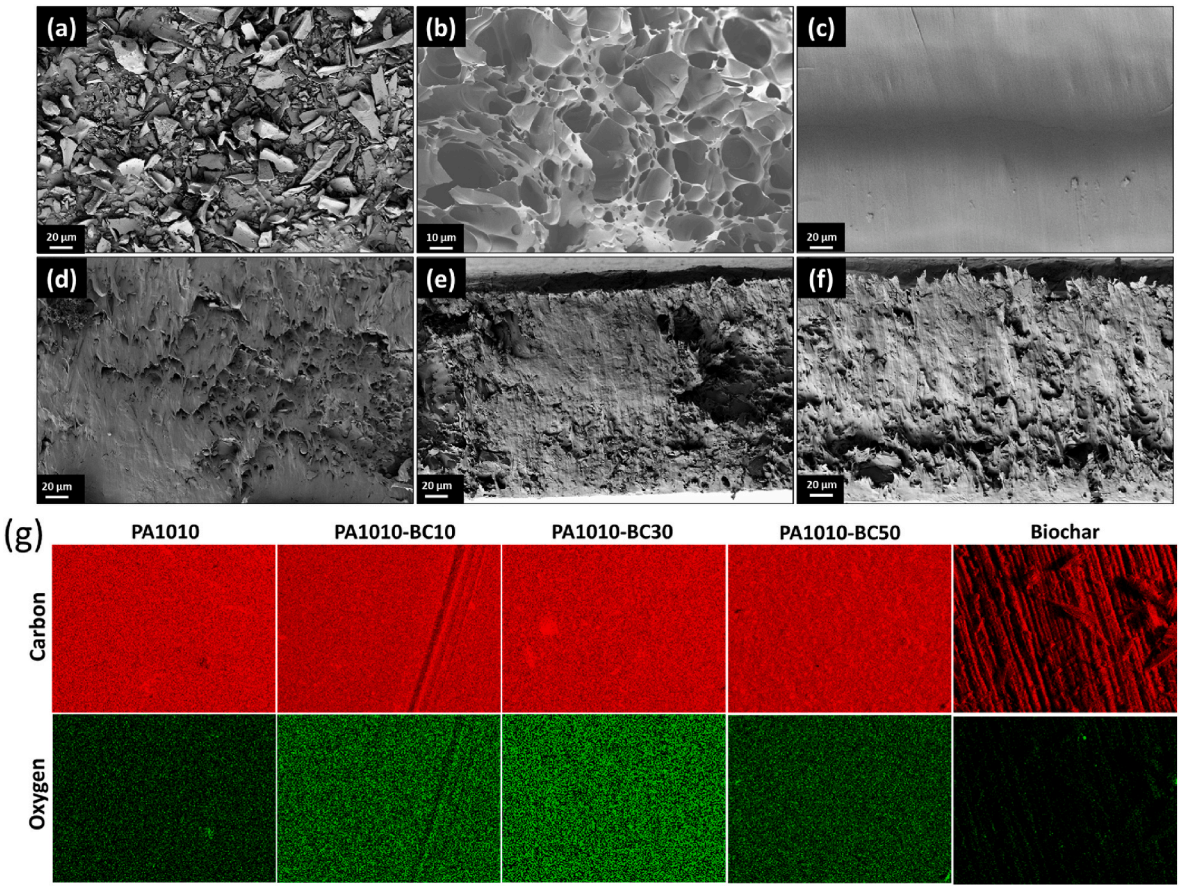

Fig. 3. (a) and (b) SEM images from the surface of biochar. SEM images from the cryofracture surface area of (c) PA1010, d) PA1010-BC10, (e) PA1010-BC30, and (f) PA1010-BC50. (g) Energy-dispersive X-ray spectroscopy (EDX) elemental mapping in PA1010, biochar, and PA1010-biochar composites.

To further support these findings, EDX analysis was conducted to examine the elemental distribution in the composites. Fig. 3g presents the elemental mapping of carbon and oxygen in PA1010, biochar, and their composites, while the elemental quantification is provided in Fig. S2. As expected, pure PA1010 exhibited a lower carbon content (~71 %) compared to biochar (~92 %), which is highly carbonaceous. Upon increasing biochar content in the biocomposites, the carbon concentration increased systematically (73.2 %, 77.6 %, and 82 % for PA1010-BC10, PA1010-BC30, and PA1010-BC50, respectively), aligning well with theoretical predictions. The corresponding oxygen content decreased accordingly (from 9.5 % in pure PA1010 to 9.25 %, 8.75 %, and 8.25 % in the respective composites), reinforcing the successful integration of biochar within the polymer matrix. The homogeneous distribution of carbon and oxygen in the EDX maps further confirms the excellent dispersion of biochar throughout the PA1010 matrix without significant agglomeration.

3.1.3. Mechanical properties

The mechanical properties of composites play a pivotal role in determining their suitability and performance across various practical applications. Therefore, the tensile properties, bending performance, and impact strength of the PA1010 and corresponding biocomposites were measured and discussed, with the results illustrated in Fig. 4. Pure PA1010 demonstrated high elongation (240 %), with a tensile strength of 38.5 ± 2.5 MPa and a tensile modulus of 1015 ± 40 MPa, consistent with the literature for pure PA1010 (Hernández-García et al., 2023; Lu et al., 2017). The addition of biochar particles improved both tensile strength and modulus while reducing elongation at break. In the biocomposite with the highest biochar content (PA1010-BC50), the tensile modulus and strength increased to 2150 ± 40 MPa and 55.5 ± 3.2 MPa, respectively, reflecting a 110 % and 44 % improvement over the pure matrix. However, elongation at break dropped to 6 %.

These results show that biochar particles reinforced the biocomposite, enhancing tensile strength and modulus. Biochar's high stiffness and strength properties, when uniformly dispersed within the polymer matrix, act as a filler material, reinforcing the matrix and resisting deformation under tensile stress. This increases both tensile strength and modulus. However, elongation at break decreased due to biochar's rigidity, which restricts polymer chain mobility and limits elongation under stress. Additionally, biochar's particle size and porosity can cause localized stress concentrations, leading to premature failure and reduced ductility. This phenomenon is common in reinforced composites, where the reinforcing agents limit plastic deformation (Abidnejad et al., 2025; Fazeli et al., 2024; Raja et al., 2024; Raja and Devarajan, 2025). Furthermore, biochar may interfere with crystallization, making the material less ductile overall.

Other studies have reported similar findings. Rajendran et al. (2024) observed a notable increase in the tensile strength of polyester composites filled with biochar. Similarly, Koriema et al. (Koriem et al., 2023) noted a significant enhancement in the tensile strength of nitrile butadiene rubber (NBR) composites due to increased hydrogen bonding between carbonyl groups in the NBR compounds. Additionally, a considerable increase in tensile modulus was reported for the epoxy resin filled with biochar derived from maple trees (Giorcelli et al., 2019). It has also been confirmed that increasing biochar filler loading enhances the stiffness of the PLA composites (Mozrall et al., 2023; Zhang et al., 2023).

A three-point bending test was conducted to evaluate the biocomposites' stiffness and strength further. Results, shown in Fig. 4b, reveal significant improvements in flexural modulus and strength with

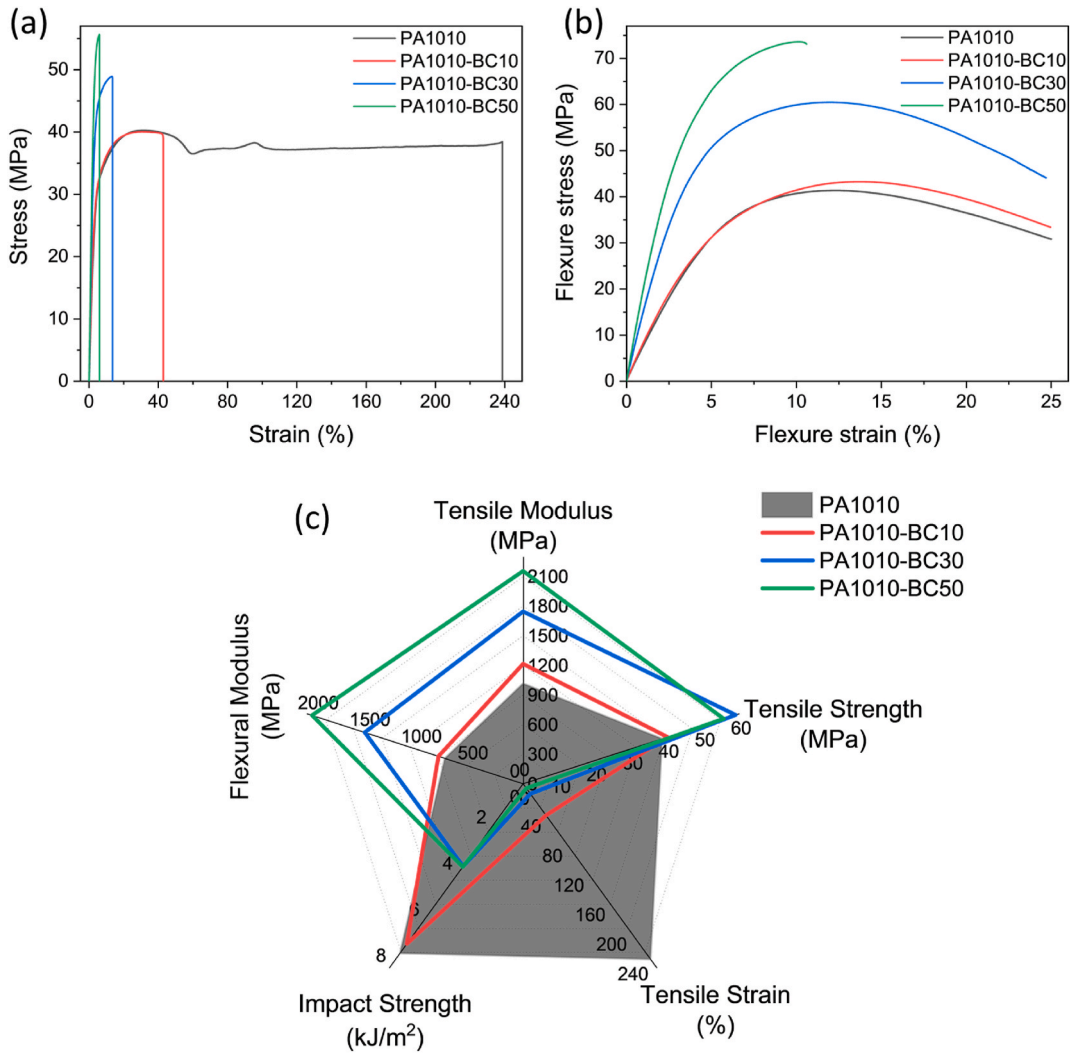

Fig. 4. Typical (a) tensile stress-strain and (b) bending curves. (c) The comparison between different mechanical properties.

increasing biochar loading. Specifically, the flexural strength increased from 40.5 ± 1.1 MPa in PA1010 to 73.8 ± 2.0 MPa in PA1010-BC50, while the flexural modulus rose from 760 ± 20 MPa to 2050 ± 35 MPa. These improvements can be attributed to biochar's reinforcement properties, its uniform dispersion within the PA1010 matrix, and its ability to enhance stress distribution during bending. Biochar's high aspect ratio and surface area facilitate strong bonding with the polymer matrix, improving stress transfer and enhancing mechanical properties (Cho et al., 2021; Rong et al., 2023). These improvements suggest that PA1010/biochar biocomposites are promising for load-bearing applications (Shahnaz et al., 2024).

Finally, an impact test was performed to assess the material's energy absorption capacity, reflecting its toughness. The results, shown in Fig. 4c, indicate that pure PA1010 exhibited the highest impact strength at 7.3 ± 0.5 kJ/m^2. In contrast, the impact strength of the biochar-containing biocomposites decreased, with PA1010-BC50 showing a reduction to 3.6 ± 0.2 kJ/m^2, a 50 % drop compared to the pure matrix. The addition of biochar seems to disrupt the biocomposite's ability to absorb and dissipate energy during impact, likely due to changes in the microstructure and potential interfacial interactions between the biochar and polymer matrix. As a result, the biocomposite's toughness and resilience under dynamic loading are reduced.

3.1.4. Thermal decomposition of biocomposites

The thermal decomposition behavior of both pure PA1010 and the developed biocomposites was examined using TGA. The corresponding plots are shown in Fig. 5, and the relevant data is summarized in Table 1. Pure PA1010 exhibited exceptional thermal stability below 400 °C, demonstrating only a minor weight change of less than 1 %. However, upon further temperature escalation, it underwent complete thermal decomposition within the range of 400 °C–550 °C, consistent with findings from prior research (Quiles-Carrillo et al., 2019; Tang et al., 2023). In contrast, biochar exhibited robust thermal stability within the tested temperature range of 30 °C–800 °C, experiencing only a minor weight loss of 10 %. This resilience can be attributed to biochar's high carbon content and structural integrity. Notably, the incorporation of biochar markedly enhanced the thermal stability of the PA1010 matrix, as evidenced by a significant increase in thermal decomposition temperatures. For instance, T5 %, T10 %, and Tmax shifted from 417 °C, 430 °C, and 460 °C in PA1010 to 425 °C, 450 °C, and 474 °C in PA1010-BC50, respectively. These findings are consistent with similar observations reported for biochar-reinforced thermoplastic matrices, including PLA (Yiga et al., 2023; Zhang et al., 2024), HDPE (Kane and Ryan, 2022; Zhang et al., 2020b), PP (Alghyamah et al., 2021; Luo et al., 2022; Mohammed et al., 2022), and PA (Baniasadi et al., 2023a; Nisa et al., 2023).

The improved thermal stability of PA1010 upon biochar incorporation can be attributed to several factors. Firstly, the high surface area and porous structure of biochar act as insulating barriers, increasing thermal resistance and delaying decomposition. Additionally, biochar

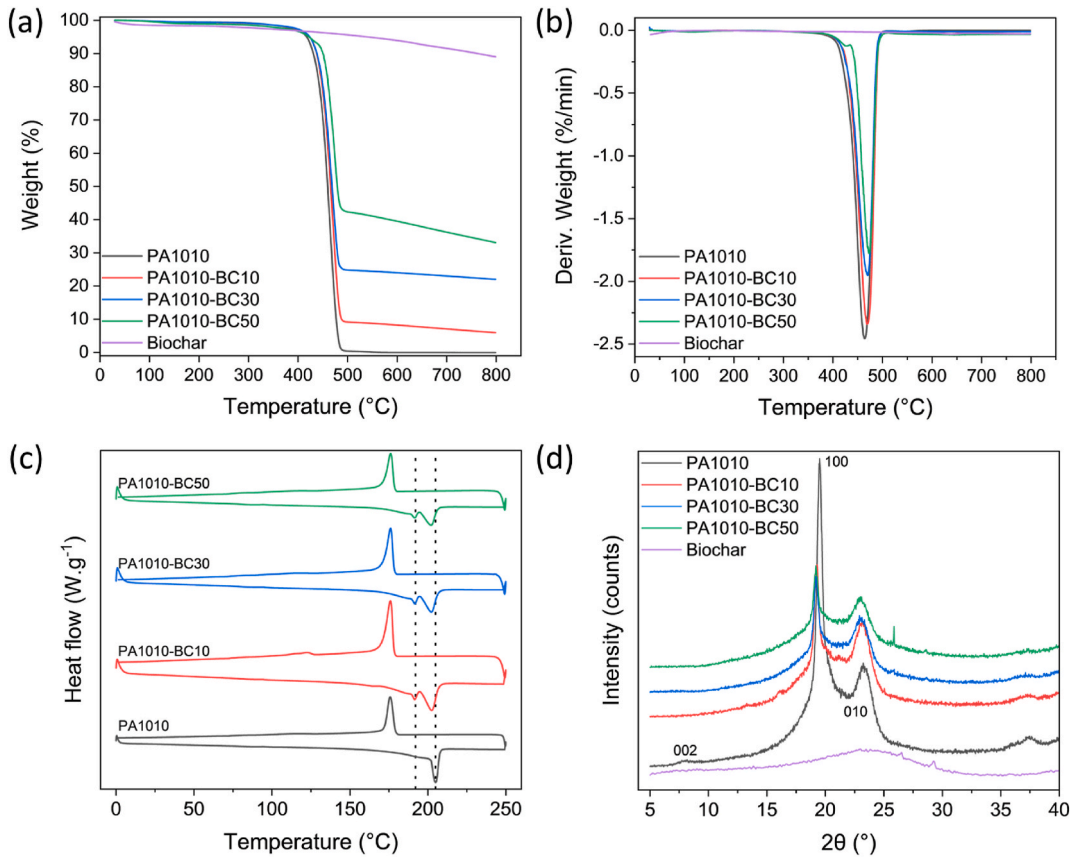

Fig. 5. (a) TGA and (b) DTG thermograms of pure PA1010, biochar, and biocomposites. (c) DSC curves and (d) XRD patterns of pure PA1010 and biocomposites.

Table 1
Thermal decomposition temperatures and residue material at 800 °C (the data are extracted for TGA and DTG plots).

Sample	$T_{5\ \%}$ (°C)	$T_{10\ \%}$ (°C)	T_{max} (°C)	Residue at 800 °C (%)
Biochar	422	763	–	89
PA1010	417	430	460	0
PA1010-BC10	423	437	468	5.9
PA1010-BC30	425	437	468	22
PA1010-BC50	425	450	474	33

enhances mechanical stability by reinforcing the polymer matrix, reducing polymer chain mobility and the likelihood of thermal degradation. Moreover, biochar can adsorb volatile decomposition products, limiting their release and mitigating degradation reactions. While biochar can exhibit catalytic properties that accelerate thermal decomposition at high temperatures, this effect was not observed in our study, likely due to the specific biochar type, surface characteristics, or its interaction with PA1010.

Table 2
Crystallization temperatures, phase change enthalpies, crystallinity, and glass transition temperature of the pure PA1010 and the developed biocomposites.

Sample	T_m (°C)	T_c (°C)	ΔH_m (J/g)	ΔH_c (J/g)	χ_c (%)	T_g (°C)
PA1010	205	176	86	57	35.2	69
PA1010-BC10	204	176	42	47	19.1	77
PA1010-BC30	203	176	36	37	21	70
PA1010-BC50	203	176	29	29	23.8	72

3.1.5. *Crystallinity of biocomposites*

DSC thermograms were employed to investigate the impact of biochar on the crystallinity of the PA1010 matrix. The DSC plots are depicted in Fig. 5c. Pertinent data, including the melting temperature and enthalpy, as well as the crystallization temperature and enthalpy, are summarized in Table 2. PA1010 exhibited a dominant endothermic peak at 203 °C, corresponding to its melting point, and a prominent exothermic peak at 176 °C, assigned to its crystallization temperature, consistent with the values reported in the literature for PA1010 (Ye et al., 2023). In contrast to other reports (Hernández-García et al., 2023; Pinto et al., 2023), no additional peaks were detected within the test temperature range, indicating the presence of one crystalline phase, namely, a highly homogeneous structure devoid of impurities or phase transitions, most likely the alpha crystalline phase (Baniasadi et al., 2021a, 2021b). Both T_m and T_c remained essentially unchanged upon the introduction of biochar, implying that the incorporation of biochar does not significantly alter the thermal properties of the PA1010 matrix.

Nevertheless, the crystallinity of PA1010 decreased from 35 % to 19 % after introducing 10 wt% biochar, possibly due to interference from the biochar particles within the PA1010 matrix, which hindered the formation of ordered crystalline structures. Another contributing factor could be the interaction between the biochar particles and the polyamide, which disrupts the packing arrangement of the polymer molecules and impedes the formation of crystalline regions. Notably, increasing the biochar concentration to 30 wt% and 50 wt% resulted in a marginal increase in crystallinity. This could be attributed to the greater presence of biochar, which may act as a more effective nucleating agent, promoting the formation of crystalline structures within the matrix. Additionally, the enhanced interaction between the biochar particles and polyamide chains at higher concentrations may improve the alignment and packing of the polymer molecules, fostering the formation of larger and more ordered crystalline regions, thereby increasing the

overall crystallinity.

XRD patterns were employed to further examine the crystalline structure of PA1010 and its biochar composites, as shown in Fig. 5d. The pure PA1010 sample exhibited sharp and well-defined diffraction peaks at 2θ values of 8.2°, 19.9°, and 23.9°, corresponding to the (002), (100), and (010) planes, respectively (Wang et al., 2019). These peaks confirm the crystalline nature of PA1010, consistent with the α-phase of polyamide crystals commonly observed in similar materials. The absence of additional peaks or shoulders indicates a homogeneous crystalline structure (Baniasadi et al., 2024), showing the dominance of a single crystalline phase, which agrees with the DSC results. In the case of biochar, a broad and diffuse peak around 2θ = 23° was observed due to the abundance of amorphous carbon (Ye et al., 2024). Upon incorporation of biochar in the polymer matrix, the XRD patterns of the composites retained the major peaks of PA1010, indicating that the fundamental crystalline structure was preserved. However, the broad, diffuse peak associated with biochar's amorphous nature was less pronounced in the composites, indicating that the biochar interferes with the crystalline packing of PA1010 at low concentrations. This interference likely causes the reduction in crystallinity, as seen with the 10 wt% biochar composite, where the crystallinity decreased from 35 % to 19 %. At higher biochar concentrations (30 wt% and 50 wt%), the crystallinity of the composites marginally increased, possibly due to biochar acting as a nucleating agent, facilitating the formation of more ordered crystalline structures. This suggests that higher biochar content enhances the interaction between biochar particles and polyamide chains, improving alignment and promoting crystallization.

3.1.6. Dynamic mechanical analysis

DMA was employed to investigate the viscoelastic behavior of PA1010 and the developed biocomposites, providing insights into the interactions between the biochar and the PA1010 matrix. All samples underwent heating up to 200 °C in a multi-frequency-strain mode, and the trend of E′ as well as tan δ versus temperature was analyzed and discussed. The results, depicted in Fig. 6a–b, revealed distinctive characteristics. At low temperatures, all samples exhibited a plateau in the storage modulus, indicating a minimal change in the material stiffness within this temperature range. This suggests efficient energy storage and recovery without significant deformation, typical of a glassy state where molecular motion is restricted. However, as temperature increased, a pronounced reduction in the storage modulus was observed across all samples, signifying a transition in the material behavior. This reduction indicated a decrease in stiffness or rigidity with the rising temperature, marking the onset of a molecular motion and a transition from a glassy to a rubbery state typically associated with the material's glass transition temperature (T_g) (Siddique et al., 2021; Wan et al., 2013). The observed T_g for PA1010, approximately 69 °C, as indicated in Table 2, exhibited an increase in the biocomposites, which is attributed to various factors. Biochar particles act as nucleating agents in the PA1010 matrix, promoting a more ordered polymer structure and increasing T_g by restricting polymer chain mobility. Their surface interactions with the polymer enhance stiffness, while their high aspect ratio and surface area improve interfacial adhesion, further limiting chain movement. Additionally, biochar particles serve as physical barriers, reinforcing the matrix and creating a network-like structure that restricts polymer flow, contributing to the T_g elevation (Bardha et al., 2023; Wan et al., 2013; Zhang et al., 2020a; Zhou et al., 2024).

On the other hand, upon introducing biochar particles, a significant increase in the storage modulus, particularly below T_g, was observed. For instance, at 25 °C, the storage modulus rose from 1735 MPa to 3204 MPa in the PA1010-BC50 biocomposites, indicating enhanced stiffness and mechanical strength. This improvement can be attributed to

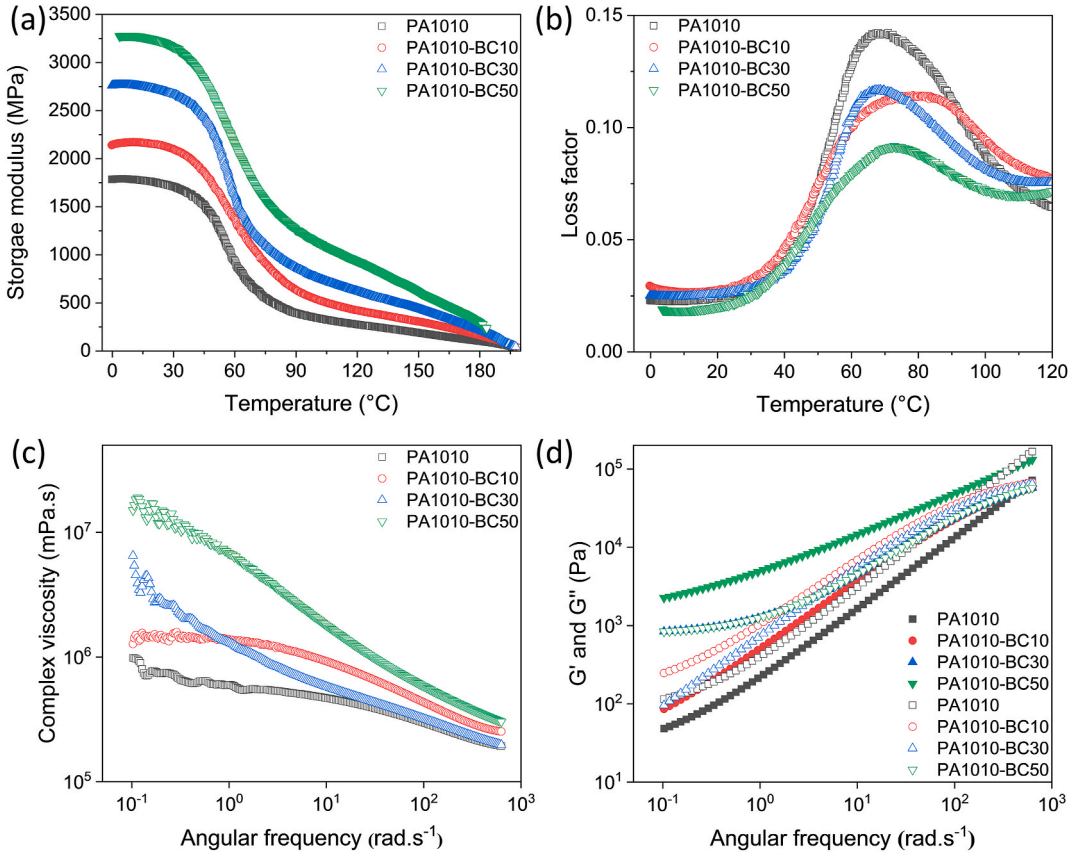

Fig. 6. Dynamic mechanical analysis results: (a) storage modulus and (b) tan δ versus temperature. Rheology results: (c) complex viscosity and (d) storage and loss moduli versus angular frequency at 1 % shear strain rate and 23 °C.

biochar's reinforcing effect within the polymer matrix, facilitated by its high aspect and surface area-to-volume ratio, which promotes strong interfacial interactions and restricts chain mobility (Alshahrani and Prakash, 2022; Raja and Devarajan, 2024; Vidal et al., 2022). Additionally, the reduction in the height of the tan δ curve, resulting from the incorporation of biochar, suggests a decrease in damping properties, further indicating the increased stiffness and rigidity of the biocomposite. This reduction in tan δ reflects the lowered internal friction at the interface between biochar and the polymer matrix, contributing to the overall enhancement of mechanical properties. This observation aligns with findings reported by Infurna et al. (2024) for PLA/biochar composites and supports the idea of restricted molecular mobility and reduced internal friction at the biochar-polymer matrix interface. Therefore, the DMA results validate the uniform dispersion of the biochar particles within the PA1010 matrix, even at a high loading of 50 wt %, and demonstrate their effective interaction, resulting in biocomposites with improved mechanical properties, characterized by higher stiffness and enhanced load-bearing capabilities.

3.1.7. Rheology properties

Rheology properties were used to further investigate polymer-filler interactions and the dispersion of biochar within the PA1010 matrix. The rheology curves, including $|\eta^*|$, G′, and G″ versus angular frequency are plotted in Fig. 6c–d. Firstly, a strain sweep test was conducted at a constant angular frequency of 10 rad/s to identify the linear viscoelastic region. The results are provided in Fig. S3. At low strain rates, all samples exhibited a constant G′ and G″, indicating a linear viscoelastic behavior. However, with a further increase in the shear strain values, both G′ and G″ began to deviate from linearity, suggesting the onset of nonlinear viscoelastic effects. Consequently, a shear strain of 1 % was chosen as a safe value to ensure that the frequency sweep test remained within the linear viscoelastic region.

Fig. 6c illustrates the trend of $|\eta^*|$ versus angular frequency. As frequency increased, viscosity decreased in all samples, indicating shear-thinning behavior. This is likely due to the disruption of intermolecular forces or polymer chain entanglements, which ease flow at higher frequencies. Additionally, biochar particles may align or reorient within the PA1010 matrix under higher frequencies, reducing resistance to flow (Baniasadi et al., 2021c; Ren et al., 2020). Shear-thinning behavior is beneficial for extrusion processes as it allows smoother material flow, reduces energy consumption, and ensures consistent product shape. However, the introduction of biochar particles increases viscosity. These particles disrupt polymer chain flow, causing entanglement or interaction with the biochar surface, which raises resistance. The high aspect ratio and surface area of the biochar particles may further enhance these interactions, increasing viscosity and introducing additional frictional forces (Mardlin et al., 2022; Nazari et al., 2024).

The PA1010-BC30 composite showed higher viscosity than the PA1010-BC10 sample at low frequencies but lower viscosity at high frequencies. At low frequencies, the increased biochar concentration leads to stronger particle-particle interactions and entanglements, raising resistance to flow and increasing viscosity. Biochar particles disrupt polymer chains more at lower shear rates, further contributing to this effect. At higher frequencies, the lower viscosity of the 30 % composite is likely due to shear-thinning behavior, where biochar particles align or reorient within the PA1010 matrix, reducing flow resistance. This effect is more pronounced in composites with higher biochar content, where particle alignment at high shear rates lowers internal friction and viscosity. In contrast, the PA1010-BC50 biocomposite exhibited the highest viscosity across the entire frequency range. The 50 wt% biochar content leads to stronger particle-particle interactions and a more extensive network within the PA1010 matrix, increasing resistance to flow. At lower frequencies, this results in greater entanglement between polymer chains and biochar particles, further raising viscosity. While shear-thinning behavior reduces viscosity at higher frequencies in some composites, the dense network and increased frictional forces in the 50 % biochar composite maintain its higher viscosity throughout.

As illustrated in Fig. 6d–G" consistently surpassed G′ across all samples, except for the biocomposite with the highest biochar content. This indicates a liquid-like behavior, where polymer chains are relaxed and exhibit significant molecular mobility, a feature typical of materials that flow easily under applied stress (Kiziltas et al., 2021; Wan et al., 2013). However, in the PA1010-BC50 biocomposite, G′ exceeded G″ across all frequencies, signaling a transition to more solid-like behavior, with increased resistance to flow and reduced molecular mobility. This shift can be attributed to the formation of an interconnected network within the polymer matrix, restricting polymer chain movement.

Both G′ and G″ increased significantly with higher biochar content, particularly at lower frequencies. This is due to the reinforcing effect of the biochar particles, which form a denser, more interconnected structure in the matrix (Lopresti et al., 2024). This enhanced structure increases resistance to deformation and improves mechanical properties, as reflected in the higher G′ and G″ values (Bai et al., 2014; Baniasadi and Seppälä, 2021; Mousavi et al., 2023) Additionally, at lower frequencies, polymer chains have more time to interact with biochar particles, forming stronger interfacial bonds that further enhance the stiffness and damping properties of the biocomposites. Thus, the increase in both G′ and G″ at lower frequencies results from improved particle dispersion and interfacial interactions within the PA1010/biochar biocomposites.

3.2. Life cycle assessment

3.2.1. LCIA results (baseline case and sensitivity analysis)

The increased incorporation of biochar as a filler in the plain PA1010 matrix was evidenced to reduce the total environmental impacts of the PA1010/biochar biocomposite granules across all the studied impact categories – carbon footprint, acidification, eutrophication (terrestrial, freshwater, and marine), as well as land use, respectively. Further, the magnitude of the total reductions per each impact category (excluding the eutrophication of freshwater) was slightly increased upon the deduction of the sequestered CO_2 and the application of green electricity in SA1, as evidenced in Table 3. These observed reductions can majorly be attributed to the progressive replacement of the international cultivation of castor beans and the production of PA1010 granules with the locally produced wood chips-derived biochar, which possessed substantially lower impacts than these two other raw materials. As an example, in the present study, the carbon footprint of biochar was found to range between 0.01 and 0.5 kg CO_2 eq./kg of biocomposite granules, the exact value depending on the biochar content and the type of case – baseline case or sensitivity analysis, respectively. Further, the lower impacts of SA1 can be reasoned to be derived from the reduced use of fossil-based resources to generate green electricity (Li et al., 2022). The interpreted LCIA results are also succinctly presented in Figs. 7 and 8 regarding the baseline case and SA1, respectively.

The preceding reasoning can also be supported by other types of data. In more detail, upon the addition of biochar up to 50 wt%, all the environmental impacts caused by the biocomposite granules were decreased by 50 % (in the case of castor beans and PA1010 granules) and

Table 3
A compilation of the total reductions in the impact categories under analysis for the baseline case and SA1, respectively.

Impact categories	Baseline[a]	SA1[a]	Baseline[b]	SA1[b]
Carbon footprint	43 %	49 %	**58 %**	**65 %**
Acidification	47 %	49 %	47 %	49 %
Eutrophication (terrestrial)	48 %	49 %	48 %	49 %
Eutrophication (freshwater)	50 %	50 %	50 %	50 %
Eutrophication (marine)	48 %	50 %	48 %	50 %
Land use	46 %	47 %	46 %	47 %

[a] Without the sequestered CO_2 in biochar.
[b] With the sequestered CO_2 in biochar.

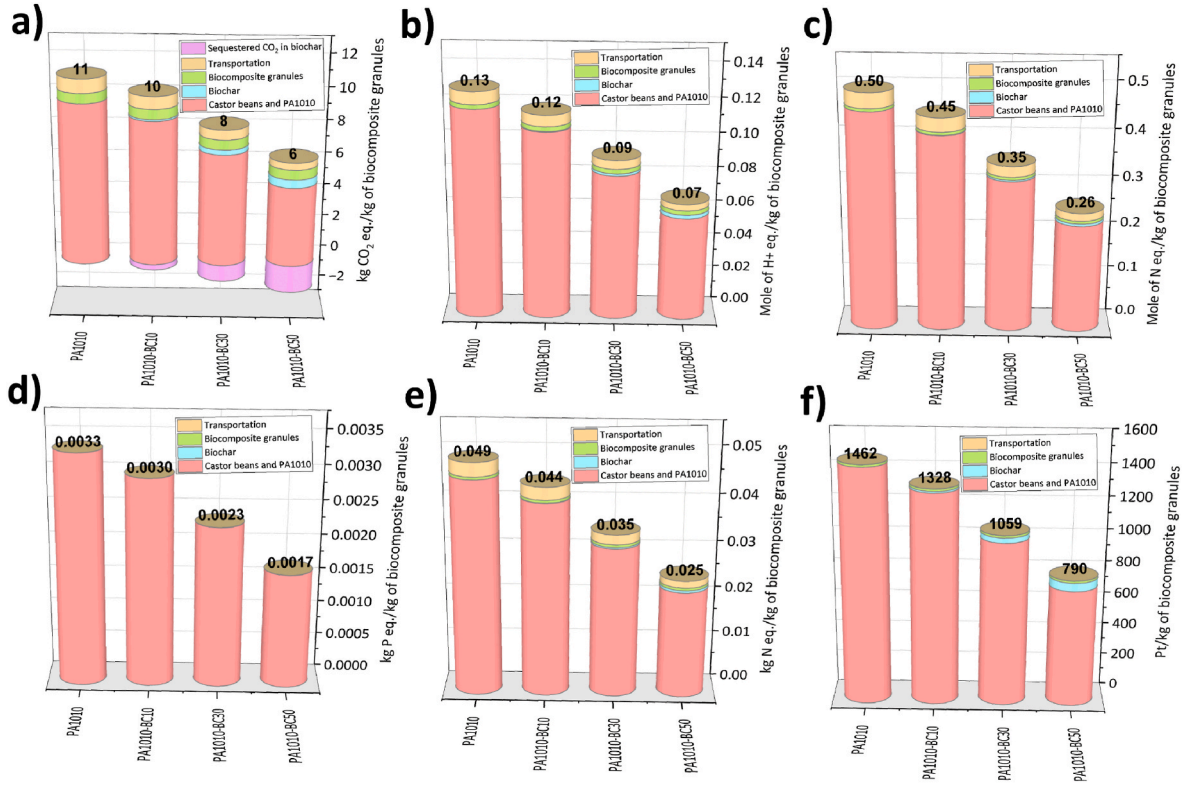

Fig. 7. LCIA results of the baseline case: (a) carbon footprint, (b) acidification, (c) eutrophication (terrestrial), (d) eutrophication (freshwater), (e) eutrophication (marine), and (f) land use.

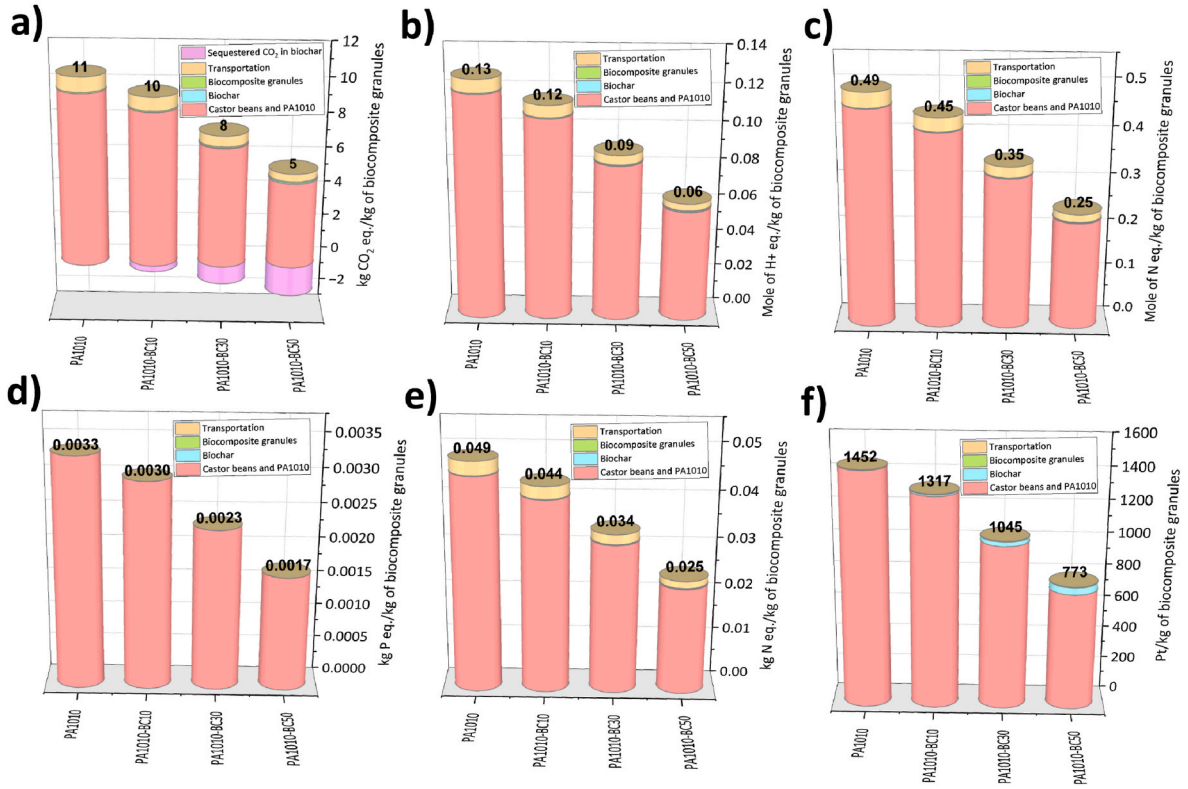

Fig. 8. LCIA results of SA1: (a) carbon footprint, (b) acidification, (c) eutrophication (terrestrial), (d) eutrophication (freshwater), (e) eutrophication (marine), and (f) land use.

Table 4
The process steps and their relative contributions to the overall impacts. The relative values were obtained by calculating a mean of all the relative contributions of the biocomposite granules across all the impact categories for the baseline case and SA1, respectively.

Cases	Castor beans and PA1010	Biochar	Biocomposite granules	Transportation
Baseline	91.3 %	1.4 %	2.3 %	4.3 %
SA1	94.2 %	0.6 %	0.5 %	4.3 %

46–50 % (in the case of transportation), respectively, in both baseline case and SA1. Remarkably, when the sequestered CO_2 was considered for both cases, the carbon footprint reductions were further increased from 50 % to 67 % (in terms of castor beans and PA1010 granules) compared to plain PA1010 granules. Simultaneously, the environmental impacts caused by the PA1010/biochar biocomposite granules remained constant, which indicates that the changes in the ratio of raw materials outside the laboratory do not significantly influence the performance of the laboratory-scale processes. Subsequently, the general order of contributors to the impacts (hotspots) in descending order was formulated as follows: castor beans and PA1010 granules, transportation, PA1010/biochar biocomposite granules, and biochar, the exact order of the last two contributors depending on the type of case (see Table 4 and Tables S13–S20 for the details). Notably, the datasets of castor beans and PA1010 granules were combined for the present interpretation to adhere to the guidelines set by Sphera Solutions GmbH.

The acquired results can be stated to be well aligned with the outcomes of past LCA studies, which have examined the characteristics of composites with biochar as the filler. In this regard, Kane et al. (2022), Roy et al. (2020), and Tadele et al. (2020) all found out that the production of plastic granules as a matrix raw material posed the biggest environmental impacts on the studied composites (>60 %) across all the impact categories, followed by the manufacture of these composites (25 %), and transportation (15 %) (Roy et al., 2020). Although the relatively low impacts of the laboratory-scale processes of the present study can be explained by the existing internal circulation of cooling water, leaving the electricity consumption of the laboratory equipment the major contributor to the environmental impacts caused by the biocomposite granules. Additionally, in the previous literature, the impacts related to the production of fillers were reported to be marginal (Tadele et al., 2020) or were primarily included in the carbon uptake during photosynthesis (Kane et al., 2022). In line with the findings of the present paper, Civancik-Uslu et al. (2018) also concluded that regardless of the filler type, the reductions in the environmental impacts of plastic products are proportional to the added filler content. This is attributed to the fact that fillers, with a lower environmental impact, replace the (fossil-based) materials, which are otherwise required to manufacture the composites (Civancik-Uslu et al., 2018). Similarly, Kane et al. (2022) demonstrated that the addition of biochar to the plastic matrix poses a linear relationship between the added biochar content and the resulting carbon footprint of the composite, leading to up to twice higher reductions in the carbon footprint compared to the added biochar content (when, however, the impacts caused by the growth of biomass to produce biochar was excluded from the analysis). In the same vein are also the results acquired by Baniasadi et al. (2024), indicating a progressive reduction in the composites' carbon footprint upon the integration of biochar into the neat PA12 plastic matrix.

The considerably high impacts related to the castor beans and PA1010 granules of the present study, combined with the distinctly low impacts caused by biochar, are also in alignment with the conclusions derived from the available literature (Bergman et al., 2022; Brizga et al., 2020; Pari et al., 2020). For instance, these literature sources indicated that the carbon footprint of the cultivation of castor beans and extraction of castor oil is 8.14 kg or 18.9 kg CO_2 eq./kg of castor oil extracted (the value being dependent on the farming practices and selling of the by-products) (Pari et al., 2020), while the carbon footprint of bio-based PAs ranged from slightly below 4 to closer to 10 kg CO_2 eq./kg of plastic (Brizga et al., 2020), respectively. Additionally, the carbon footprint of biochar pellets was found to be 0.27 (without forest operations) and 0.37 (with the forest operations) kg CO_2 eq./kg of biochar pellets when the transport of biochar pellets or their EoL was not included in the LCA (Bergman et al., 2022). Noteworthy, due to considerable methodological differences between the LCAs of the analyzed literature sources and the present study, the direct comparison of the composites was considered not to yield sufficiently truthful information; however, general conclusions were able to be drawn, as done in the present section.

While pyrolysis offers environmental benefits, it also involves technical and environmental trade-offs. Biochar quality and yield depend on feedstock type (e.g., moisture content, waste stream), pre-treatment, pyrolysis equipment (Zhu et al., 2022), and process parameters like temperature and residence time. Higher temperatures and shorter residence times favor bio-oil production but increase energy consumption, whereas lower temperatures with longer residence times maximize biochar yield with lower energy use (Afshar and Mofatteh, 2024; Zhu et al., 2022). Additionally, higher temperatures promote secondary reactions, reducing biochar and bio-oil yields (Zhu et al., 2022).

Large-scale pyrolysis is more energy-efficient and has a lower carbon footprint than small-scale pyrolysis, which can cause more air pollution and particulate emissions (Zhu et al., 2022), potentially undermining CO_2 sequestration benefits. The 500 °C pyrolysis temperature, recommended for lignocellulosic feedstock (Zhu et al., 2018, 2022), was used in this study to ensure successful biochar production while maintaining CO_2 sequestration benefits. Lignocellulosic feedstocks, especially agricultural residues, are more environmentally friendly than alternatives like sludge or pig manure. Energy consumption can be further reduced by capturing pyrolysis gas energy (up to 28 %) and including biochar use and its EoL in the LCA (Afshar and Mofatteh, 2024). Scaling the laboratory process to an industrial scale would likely further reduce the carbon footprint. This aligns with findings from Tsalidis and Korevaar (2022), which show that laboratory-scale torrefaction has a significantly higher carbon footprint and terrestrial acidification than industrial-scale processes. Thus, scaling up would likely reinforce the study's conclusions, highlighting biochar as an effective filler for reducing the carbon footprint and agricultural impacts of bio-based PA1010 plastic.

3.2.2. *Comparison with commercial plastics and early-stage composites*

To validate the LCIA results, PA/biochar biocomposites were compared with early-stage PA-based composites, as well as commercial and sustainable plastics made from bio-based or recycled materials or produced using renewable energy. The PA1010-BC50 biocomposite, with 50 wt% biochar was selected for comparison due to its lowest environmental impacts. Commercial plastics and early-stage composites were chosen based on similar functional units, system boundaries, and impact categories. Methodological details and comparisons with PA1010-BC50 are presented in Table S6 and Table S21. Only carbon footprint as well as freshwater and marine eutrophication were considered for comparison due to differences in impact assessment methods.

After analyzing Table 5, key factors influencing the LCIA results include the feedstock origin (main vs. side/waste stream), type of filler and plastic matrix (bio- vs. fossil-based), electricity grid mix (renewable, fossil-based, or mixed), and the number of optimized manufacturing processes. For the PA12/biochar composites (#3 and #4), composite #3, using fossil-based energy, showed increased impacts across all categories despite using wood chips as a waste stream and a thermal oxidizer in pyrolysis. In contrast, switching to a fully renewable electricity grid mix in composite #4 significantly reduced all impacts (Baniasadi et al., 2024). The PA66/lignin-based carbon fiber (CF) composite (#6) showed a significantly higher carbon footprint than other composites in Table 5, primarily due to the fossil-based PA66 matrix (6.45 kg CO_2 eq./kg) and the energy-intensive production of

Table 5
A comparison of PA1010-BC50 biocomposite (baseline case and SA1) with the selected early-stage composites available in the literature. The data for the composites of PA12/biochar, PA11coPA1218/starch, and PA66/lignin-based CF were collected from Baniasadi et al. (2024), Äkräs et al. (2024), and Beaucamp et al. (2024)/Moncada et al. (2018), respectively. The sequestered CO_2 is included in the values.

Composite	Carbon footprint (kg CO_2 eq.)	Freshwater eutrophication (kg P eq.)	Marine eutrophication (kg N eq.)
#1: PA1010/biochar (50 wt%)[a]	4.73	0.0017	0.025
#2: PA1010/biochar (50 wt%)[b]	3.77	0.0017	0.025
#3: PA12/biochar (50 wt%)[c]	2.32	0.0039	0.00028
#4: PA12/biochar (50 wt%)[d]	−1.83	−0.00008	−0.00003
#5: PA11coPA1218/ starch (50 wt%)[e]	3.9	0.00065	0.011
#6: PA66/lignin-based CF (20 wt %)[f]	18.1	n.d	n.d

[a] Biofiller as a primary stream, Finnish electricity in the laboratory phase.
[b] Biofiller as a primary stream, global green electricity in the laboratory phase.
[c] Biofiller as a waste stream, fossil-based electricity, thermal oxidizer.
[d] Biofiller as a waste stream, fully renewable energy, thermal oxidizer.
[e] Biofiller as a primary stream, Finnish electricity in terms of biofiller and the laboratory phase.
[f] Biofiller as a side stream, varying electricity grid mixes.

lignin-based CFs. These were made by compounding 50 wt% bio-based TPU with 50 wt% organosolv lignin, which accounted for 56 % of the total carbon footprint (Beaucamp et al., 2024). In comparison, PA1010/biochar biocomposites (#1 and #2) outperformed the PA66/lignin-based CF (#6) in both baseline and SA1 cases, and PA1010/biochar also had lower freshwater eutrophication than PA12/biochar (#3) made with fossil-based electricity. However, further process optimizations are needed to improve the biocomposites' environmental performance, which will be discussed in section 3.2.4.

Some commercial polyamides were also chosen for comparison (Arkema, 2025; Evonik, 2024; Morão and De Bie, 2019). A direct comparison of PA1010-BC50 biocomposites with these plastics is shown in Fig. 9. Due to a lack of comparable units, only carbon footprint, acidification, and freshwater eutrophication were considered. Vestamid® Terra DS PA1010 had the highest environmental impacts, likely due to the use of standard energy and land-intensive castor bean cultivation. The PA1010-BC50 biocomposites performed better than commercial PA1010 in all impact categories and outperformed Vestamid® D PA612 and Vestamid® eCO E40 CC50 PTA in acidification and freshwater eutrophication, respectively. Vestamid® eCO L BBM PA12 excelled in all categories, benefiting from renewable or recycled materials and renewable energy. Interestingly, Vestamid® eCO E40 CC50 PTA had higher freshwater eutrophication impacts, likely due to the use of biomass-based renewable energy, which contributes significantly to eutrophication compared to other renewable sources like wind or solar (Mahmud and Farjana, 2022) (see Fig. 9).

3.2.3. Functional performance-to-impact ratio

To further evaluate the sustainability characteristics of the newly developed PA1010/biochar biocomposites, the functional performance-to-impact ratio was calculated, which core purpose was to compare the biocomposites' improvements in the mechanical properties against their observed environmental impact reductions. In this sense, as also previously reported, the incorporation of biochar in the neat PA1010 matrix resulted in significant enhancements: tensile strength increased by 44 % (from 38.5 MPa to 55.5 MPa), and tensile modulus rose by 110 % (from 1015 MPa to 2150 MPa), respectively. Simultaneously, in terms of the analyzed environmental impacts, the conducted LCA demonstrated up to 65 %, 49 %, 50 %, and 47 % impact reductions in the carbon footprint, acidification and terrestrial eutrophication, freshwater and marine eutrophication, as well as land use, respectively, which is attributed to the gradually increased biochar content in the biocomposites. The calculated functional performance-to-impact ratios for improvements in the tensile strength and modulus, relative to the reductions in each impact category, are conveniently presented in Fig. 10, which highlights each percentage point of tensile strength or modulus improvement corresponding to a reduction of 0.68–0.90 or 1.69–2.24 percentage points, respectively, in the studied environmental impacts. In conclusion, the present analysis can be argued to underscore the potential of PA1010/biochar biocomposites as more sustainable material alternatives, balancing improved mechanical performance with substantial environmental benefits.

3.2.4. Uncertainties, areas for development, and future outlook

The LCA study contains uncertainties from LCI compilation,

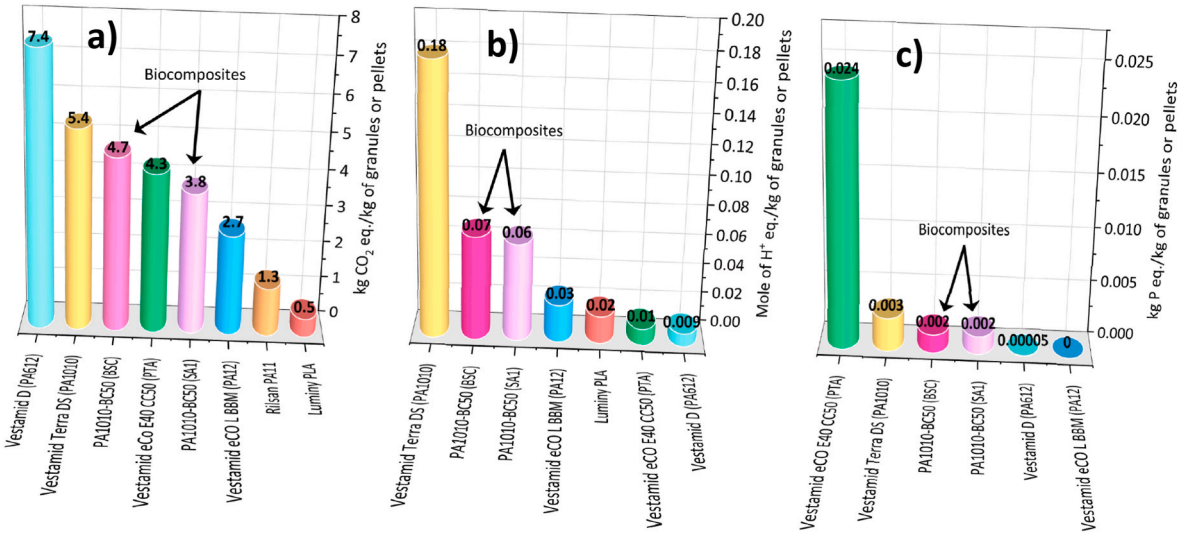

Fig. 9. A comparison of the PA1010-BC50 biocomposite (baseline case (BSC) and SA1) with the selected commercial plastics. a) Carbon footprint, b) acidification, and c) eutrophication (freshwater). Due to the lack of data or comparable units, Rilsan® PA11 was excluded from graphs b) and c) and Luminy® PLA from graph b), respectively. The presented values also include the amount of sequestered CO_2.

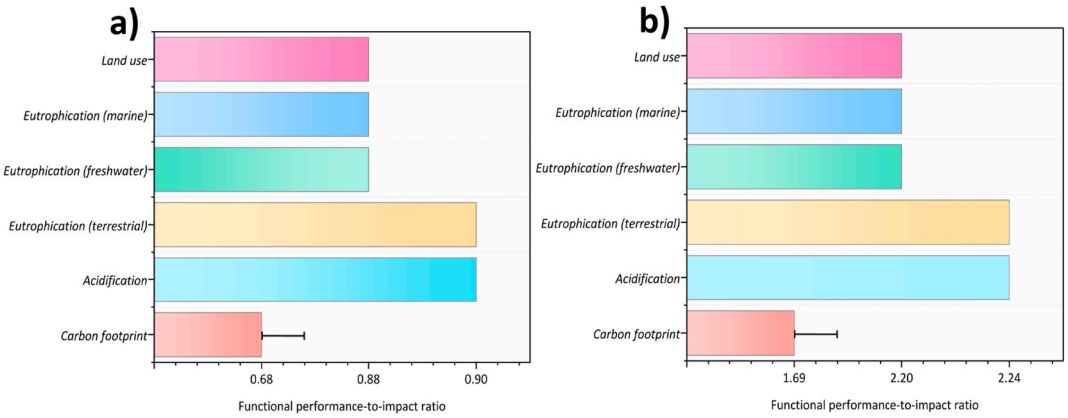

Fig. 10. Values of the calculated functional performance-to-impact ratios: a) tensile strength and b) tensile modulus per each environmental impact, respectively. In terms of the carbon footprint, both the results of the baseline case and sensitivity analysis (0.68 and 1.90, respectively) are depicted in the graphs, while in regard to other impact categories, the results of the baseline case and sensitivity analysis remain the same.

modeling practices, and assumptions (Ren, 2021). Estimations of pyrolysis furnace and extruder power, cooling water use, and equipment times, along with the use of a German dataset for PA1010 granules and estimated biochar molecular formulas, may have influenced the LCIA results. However, transport parameter variations have a minimal impact (Tadele et al., 2020; Roy et al., 2019) and pyrolysis of wood-based feedstock aligns with findings in this study (Afshar and Mofatteh, 2024).

While the LCIA results are robust due to laboratory-scale data, replacing secondary data with primary data and scaling up the process could improve accuracy (Kralisch et al., 2015; Roy et al., 2020; Tadele et al., 2020). Additionally, replacing the laboratory-scale data with the industrial one (for example, by scaling up the process setup to an industrial scale) could derive more accurate information about the environmental impacts of the PA1010/biochar biocomposites under study (Roy et al., 2020). Ultimately, after scaling up, incorporating the use and EoL phases of the biocomposites into the LCA could potentially make them carbon neutral or even carbon negative (Osman et al., 2022; Roy et al., 2019; Bergman et al., 2022).

Longer biochar sequestration improves carbon storage, and increasing plastic lifespan through design, reuse, and recycling could reduce environmental impacts (Kane et al., 2022; Meng et al., 2024). Although biochar-based composites are currently difficult to recycle (Kane et al., 2022; Roy et al., 2019), further research on their lifespan and applicability is recommended. Decarbonizing energy sources and improving material efficiency are feasible actions to reduce plastic impacts, including mitigating impacts from castor bean cultivation and using more decarbonized PA1010 synthesis pathways (Pari et al., 2020; Meng et al., 2024). The LCIA results provide a foundation for process optimization and environmental impact assessment. After process optimizations, ex-ante LCA can be used to evaluate the biocomposites' impacts at an industrial scale, addressing limitations of laboratory-scale LCAs, such as energy efficiency and scalability issues (Piccinno et al., 2015; Recupido et al., 2023).

4. Conclusions

In this study, we conducted a comprehensive experimental and methodological investigation of novel PA1010/biochar biocomposites, systematically analyzing their physical properties and sustainability aspects. SEM analysis confirmed excellent compatibility and interface adhesion between the biochar particles and the PA1010 matrix, with uniform dispersion observed throughout the matrix. Mechanical testing revealed significant improvements in tensile strength (from 38.5 MPa to 55.5 MPa), tensile modulus (from 1015 MPa to 2150 MPa), and flexural strength (from 40.5 MPa to 73.8 MPa) with increasing biochar content, demonstrating the reinforcing effect of biochar and enhanced interfacial interactions. Thermal decomposition studies showed an increase in the thermal stability of the biocomposites, along with a reduction in crystallinity due to the interference in polymer matrix formation and nucleation site effects. DMA and rheology studies further corroborated these findings, showing enhanced stiffness and resistance to flow in the biocomposites. Additionally, LCA results demonstrated a reduction in environmental impacts, with up to a 65 % decrease in carbon footprint when biochar replaced PA1010 granules. These results indicate the potential of biochar-reinforced PA1010 biocomposites for more sustainable applications, such as in the automotive, construction, and packaging industries, where enhanced mechanical properties and reduced environmental impact are of paramount importance. Looking forward, this work provides a foundation for further process optimizations and advanced *ex-ante* LCA assessments. The promising mechanical and thermal properties, coupled with the environmental benefits of biochar, suggest that these biocomposites can play a crucial role in sustainable material design. Future research will focus on scaling up the production process and exploring additional applications, such as in smart materials and high-performance engineering components. The integration of biochar into biopolymer matrices aligns with the growing demand for environmentally friendly materials, and this study contributes to the ongoing efforts to reduce industrial carbon footprints, providing a positive impact on society by promoting more sustainable and eco-friendly material solutions.

CRediT authorship contribution statement

Hossein Baniasadi: Writing – review & editing, Writing – original draft, Visualization, Project administration, Methodology, Investigation, Formal analysis, Data curation, Conceptualization. **Laura Äkräs:** Writing – review & editing, Writing – original draft, Visualization, Software, Methodology, Investigation, Formal analysis, Data curation, Conceptualization. **Zoe Paganelli:** Investigation, Formal analysis. **Nele Dammann:** Investigation, Formal analysis. **Roozbeh Abidnejad:** Investigation. **Sami Lipponen:** Investigation. **Frans Silvenius:** Methodology. **Marjatta Vahvaselkä:** Writing – review & editing, Conceptualization. **Hannu Ilvesniemi:** Writing – review & editing, Conceptualization. **Jukka Seppälä:** Writing – review & editing, Resources, Funding acquisition. **Jukka Niskanen:** Writing – review & editing, Supervision, Resources, Project administration, Funding acquisition.

Declaration of competing interest

The authors declare that they have no known competing financial interests or personal relationships that could have appeared to influence

the work reported in this paper.

Acknowledgment

This work was supported by the Research Council of Finland, with grants No. 327248 (ValueBiomat) and 327865 (Bioeconomy), respectively.

Appendix A. Supplementary data

Supplementary data to this article can be found online at https://doi.org/10.1016/j.envres.2025.121446.

Data availability

Data will be made available on request.

References

Abidnejad, R., Baniasadi, H., Fazeli, M., Lipponen, S., Kontturi, E., Rojas, O.J., Mattos, B. D., 2025. High-fiber content composites produced from mixed textile waste: balancing cotton and polyester fibers for improved composite performance. Int. J. Biol. Macromol. 292, 139227. https://doi.org/10.1016/j.ijbiomac.2024.139227.

Afshar, M., Mofatteh, S., 2024. Biochar for a sustainable future: environmentally friendly production and diverse applications. Results in Engineering 23, 102433. https://doi.org/10.1016/j.rineng.2024.102433.

Äkräs, L., Silvenius, F., Baniasadi, H., Vahvaselkä, M., Ilvesniemi, H., Seppälä, J., 2024. A cradle-to-gate life cycle assessment of polyamide-starch biocomposites: carbon footprint as an indicator of sustainability. Clean Technol. Environ. Policy 1–16.

Alghyamah, A.A., Elnour, A.Y., Shaikh, H., Haider, S., Poulose, A.M., Al-Zahrani, S.M., Almasry, W.A., Park, S.Y., 2021. Biochar/polypropylene composites: a study on the effect of pyrolysis temperature on crystallization kinetics, crystalline structure, and thermal stability. J. King Saud Univ. Sci. 33, 101409.

Alijagic, A., Kotlyar, O., Larsson, M., Salihovic, S., Hedbrant, A., Eriksson, U., Karlsson, P., Persson, A., Scherbak, N., Färnlund, K., Engwall, M., Särndahl, E., 2024. Immunotoxic, genotoxic, and endocrine disrupting impacts of polyamide microplastic particles and chemicals. Environ. Int. 183, 108412. https://doi.org/10.1016/j.envint.2023.108412.

Alshahrani, H., Prakash, V.R.A., 2022. Mechanical, fatigue and DMA behaviour of high content cellulosic corn husk fibre and orange peel biochar epoxy biocomposite: a greener material for cleaner production. J. Clean. Prod. 374, 133931.

Ang, P., Mothe, S.R., Chennamaneni, L.R., Aidil, F., Khoo, H.H., Thoniyot, P., 2020. Laboratory-scale life-cycle assessment: a comparison of existing and emerging methods of poly (ε-caprolactone) synthesis. ACS Sustain Chem Eng 9, 669–683.

Arjona-Jaime, P., Isaacs-Páez, E.D., Nieto-Delgado, C., Chazaro-Ruiz, L.F., Rangel-Mendez, R., 2024. Insight into the effect of pressure on the CO2 capture capacity and kinetics by a biochar-ionic liquid composite. J. Environ. Chem. Eng. 12, 111804. https://doi.org/10.1016/j.jece.2023.111804.

Arkema, 2025. Arkema [WWW document]. Reducing the carbon footprint of bio-based polyamide 11 global production. URL. https://hpp.arkema.com/en/sustainability/life-cycle-assessment-carbon-foot-print. accessed 3.3.25.

Azzi, E.S., Karltun, E., Sundberg, C., 2021. Assessing the diverse environmental effects of biochar systems: an evaluation framework. J Environ Manage 286, 112154. https://doi.org/10.1016/j.jenvman.2021.112154.

Bai, J., Goodridge, R.D., Hague, R.J.M., Song, M., Okamoto, M., 2014. Influence of carbon nanotubes on the rheology and dynamic mechanical properties of polyamide-12 for laser sintering. Polym. Test. 36, 95–100.

Baniasadi, H., Abidnejad, R., Cruz, C.D., Fathi, Z., Tammela, P., Kontturi, E., Lizundia, E., 2025a. Sustainable multifunctional foams for cold-chain packaging: stabilizing polyethylene glycol with cellulose and pomegranate peel for antibacterial protection and temperature control. Sustainable Materials and Technologies 43, e01312. https://doi.org/10.1016/j.susmat.2025.e01312.

Baniasadi, H., Borandeh, S., Seppälä, J., 2021a. High-performance and biobased polyamide/functionalized graphene oxide nanocomposites through in situ polymerization for engineering applications. Macromol. Mater. Eng. 306, 2100255. https://doi.org/10.1002/MAME.202100255.

Baniasadi, H., Chatzikosmidou, D., Seppälä, J., 2023a. Innovative integration of pyrolyzed biomass into polyamide 11: sustainable advancements through in situ polymerization for enhanced mechanical, thermal, and additive manufacturing properties. Addit. Manuf. 78, 103869. https://doi.org/10.1016/j.addma.2023.103869.

Baniasadi, H., Fathi, Z., Lizundia, E., Cruz, C.D., Abidnejad, R., Fazeli, M., Tammela, P., Kontturi, E., Lipponen, J., Niskanen, J., 2025b. Development and characterization of pomegranate peel extract-infused carboxymethyl cellulose composite films for functional, sustainable food packaging. Food Hydrocoll. 158, 110525. https://doi.org/10.1016/j.foodhyd.2024.110525.

Baniasadi, H., Liizundia, E., Paganelli, Z., Dammann, N., Välinen, L., Seppälä, J., Niskanen, J., 2024. Structure-property correlations study in biochar-enhanced polyamide composites for sustainable materials development. Compos. B Eng. 286, 111809. https://doi.org/10.1016/j.compositesb.2024.111809.

Baniasadi, H., Lipponen, S., Asplund, M., Seppälä, J., 2023b. High-concentration lignin biocomposites with low-melting point biopolyamide. Chem. Eng. J. 451, 138564. https://doi.org/10.1016/j.cej.2022.138564.

Baniasadi, H., Madani, Z., Mohan, M., Vaara, M., Lipponen, S., Vapaavuori, J., Seppälä, J.V., 2023c. Heat-induced actuator fibers: starch-containing biopolyamide composites for functional textiles. ACS Appl. Mater. Interfaces 15, 48584–48600.

Baniasadi, H., Seppälä, J., 2021. Novel long-chain aliphatic polyamide/surface-modified silicon dioxide nanocomposites: in-situ polymerization and properties. Mater. Today Chem. 20, 100450. https://doi.org/10.1016/J.MTCHEM.2021.100450.

Baniasadi, H., Trifol, J., Lipponen, S., Seppälä, J., 2021b. Sustainable composites of surface-modified cellulose with low–melting point polyamide. Mater. Today Chem. 22, 100590.

Baniasadi, H., Trifol, J., Ranta, A., Seppälä, J., 2021c. Exfoliated clay nanocomposites of renewable long-chain aliphatic polyamide through in-situ polymerization. Compos. B Eng. 211, 108655.

Bardha, A., Prasher, S., Villarta, J., Francis, M.S., Khirpin, C.Y., Mehlem, J.J., Dumont, M.-J., 2023. Nut shell and grain husk waste biochar as carbon black replacements in styrene-butadiene rubber composites and improvements through steam activation. Ind. Crops Prod. 203, 117180. https://doi.org/10.1016/j.indcrop.2023.117180.

Beaucamp, A., Muddasar, M., Culebras, M., Collins, M.N., 2024. Sustainable lignin-based carbon fibre reinforced polyamide composites: production, characterisation and life cycle analysis. Compos. Commun. 45, 101782. https://doi.org/10.1016/j.coco.2023.101782.

Bergman, R., Sahoo, K., Englund, K., Mousavi-Avval, S.H., 2022. Lifecycle assessment and techno-economic analysis of biochar pellet production from forest residues and field application. Energies 15, 1559.

Brassard, P., Godbout, S., Hamelin, L., 2021. Framework for consequential life cycle assessment of pyrolysis biorefineries: a case study for the conversion of primary forestry residues. Renew. Sustain. Energy Rev. 138, 110549. https://doi.org/10.1016/j.rser.2020.110549.

Brizga, J., Hubacek, K., Feng, K., 2020. The unintended side effects of bioplastics: carbon, land, and water footprints. One Earth 3, 45–53. https://doi.org/10.1016/j.oneear.2020.06.016.

Cho, B.-G., Ram Joshi, S., Hun Han, J., Kim, G.-H., Park, Y.-B., 2021. Interphase strengthening of carbon fiber/polyamide 6 composites through mixture of sizing agent and reduced graphene oxide coating. Compos Part A Appl Sci Manuf 149, 106521. https://doi.org/10.1016/j.compositesa.2021.106521.

Civancik-Uslu, D., Ferrer, L., Puig, R., Fullana-i-Palmer, P., 2018. Are functional fillers improving environmental behavior of plastics? A review on LCA studies. Science of the total environment 626, 927–940.

Costamagna, M., Massaccesi, B.M., Mazzucco, D., Baricco, M., Rizzi, P., 2023. Environmental assessment of the recycling process for polyamides - polyethylene multilayer packaging films. Sustainable Materials and Technologies 35, e00562. https://doi.org/10.1016/j.susmat.2022.e00562.

Cucurachi, S., Van Der Giesen, C., Guinée, J., 2018. Ex-ante LCA of emerging technologies. In: Procedia CIRP. Elsevier B.V., pp. 463–468. https://doi.org/10.1016/j.procir.2017.11.005

Das, C., Tamrakar, S., Kiziltas, A., Xie, X., 2021. Incorporation of biochar to improve mechanical, thermal and electrical properties of polymer composites. Polymers 13, 2663.

Evonik, 2024. Evonik [WWW document]. Evonik's plastics database 2024. URL. https://www.plastics-database.com. accessed 3.3.25.

Fazeli, M., Jayaprakash, S., Baniasadi, H., Abidnejad, R., Lipponen, J., 2024. Recycled carbon fiber reinforced composites: enhancing mechanical properties through co-functionalization of carbon nanotube-bonded microfibrillated cellulose. Compos Part A Appl Sci Manuf 180, 108097. https://doi.org/10.1016/j.compositesa.2024.108097.

Francis, J.C., Nighojkar, A., Kandasubramanian, B., 2023. Relevance of wood biochar on CO2 adsorption: a review. Hybrid Advances 3, 100056. https://doi.org/10.1016/j.hybadv.2023.100056.

Fu, X., Zhao, X., Li, L., Zhou, C., Dong, X., Wang, D., Yang, G., 2020. Graphene/polyamide-6 microsphere composites with high electrical and mechanical performance. Composites Part C: Open Access 2, 100043. https://doi.org/10.1016/j.jcomc.2020.100043.

George, J., Azad, L.B., Poulose, A.M., An, Y., Sarmah, A.K., 2019. Nano-mechanical behaviour of biochar-starch polymer composite: investigation through advanced dynamic atomic force microscopy. Compos Part A Appl Sci Manuf 124, 105486.

Giorcelli, M., Khan, A., Pugno, N.M., Rosso, C., Tagliaferro, A., 2019. Biochar as a cheap and environmental friendly filler able to improve polymer mechanical properties. Biomass Bioenergy 120, 219–223. https://doi.org/10.1016/j.biombioe.2018.11.036.

Hernández-García, E., Pacheco-Romeralo, M., Pascual-Ramírez, L., Vargas, M., Torres-Giner, S., 2023. Synthesis and characterization of polyamide 1010 and evaluation of its cast-extruded films for meat preservation. Food Packag. Shelf Life 36, 101058. https://doi.org/10.1016/j.fpsl.2023.101058.

Hopkinson, L., James, P., Lenegan, N., McGrath, T., Tait, M., 2011. Energy consumption of university laboratories: detailed results from S-Lab audits. Bradford: S-Lab. My Green Lab 1–58.

Iliescu, O., 2023. Assessment of Biomass Uses in Helsinki for Biochar and Bioenergy Production for Climate Change Mitigation.

Infurna, G., Botta, L., Ingargiola, I., Maniscalco, M., Caputo, G., Dintcheva, N.T., 2024. Biochar from digestate pyrolysis as a filler for biopolymer blends: effect of blend composition. J. Polym. Environ. 32, 1921–1936.

Kane, S., Ryan, C., 2022. Biochar from food waste as a sustainable replacement for carbon black in upcycled or compostable composites. Composites Part C: Open Access 8, 100274. https://doi.org/10.1016/j.jcomc.2022.100274.
Kane, S., Van Roijen, E., Ryan, C., Miller, S., 2022. Reducing the environmental impacts of plastics while increasing strength: biochar fillers in biodegradable, recycled, and fossil-fuel derived plastics. Composites Part C: Open Access 8, 100253. https://doi.org/10.1016/j.jcomc.2022.100253.
Kiziltas, A., Liu, W., Tamrakar, S., Mielewski, D., 2021. Graphene nanoplatelet reinforcement for thermal and mechanical properties enhancement of bio-based polyamide 6, 10 nanocomposites for automotive applications. Composites Part C: Open Access 6, 100177.
Koriem, A.A., Abd El-Aziz, M.E., Salem, S.R., Hussain, A.I., Turky, G., 2023. Management of agricultural waste to manufacture biochar: an alternative reinforcing filler for carbon black in nitrile butadiene rubber composites. J. Clean. Prod. 428, 139360. https://doi.org/10.1016/j.jclepro.2023.139360.
Kralisch, D., Ott, D., Gericke, D., 2015. Rules and benefits of life cycle assessment in green chemical process and synthesis design: a tutorial review. Green Chem. 17, 123–145.
Li, L., Lin, J., Wu, N., Xie, S., Meng, C., Zheng, Y., Wang, X., Zhao, Y., 2022. Review and outlook on the international renewable energy development. Energy and Built Environment 3, 139–157. https://doi.org/10.1016/j.enbenv.2020.12.002.
Li, Z., Guan, J., Yan, C., Chen, N., Wang, C., Liu, T., Cheng, F., Guo, Q., Zhang, X., Ye, X., Liu, Y., Shao, Z., 2023. Corn straw core/cellulose nanofibers composite for food packaging: improved mechanical, bacteria blocking, ultraviolet and water vapor barrier properties. Food Hydrocoll. 143, 108884. https://doi.org/10.1016/j.foodhyd.2023.108884.
Lopresti, F., Botta, L., Pernice, G., Garofalo, G., Gaglio, R., 2024. Influence of biochar on the properties of antibacterial PBAT/carvacrol films. J. Polym. Environ. 1–17.
Lu, Z., Wu, A., Ou, X., Zhang, S., Niu, J., Ji, S., Ling, Y., 2017. Enhanced anti-aging and mechanical properties of polyamide 1010 by sol-hydrothermal synthetic titanium dioxide-coated kaolinite addition. J. Alloys Compd. 693, 381–388. https://doi.org/10.1016/j.jallcom.2016.09.099.
Luo, W., Zhang, S., Zhang, D., Wang, T., Dong, H., Song, M., Tang, Q., Zhou, Z., 2022. Co-pyrolysis of Chinese herb residue and reused polypropylene: comparison of pyrolysis product diversification and upgrading over metal/ZSM-5 and metal/biochar catalysts. Fuel Process. Technol. 235, 107368. https://doi.org/10.1016/j.fuproc.2022.107368.
Madani, Z., Silva, P.E.S., Baniasadi, H., Vaara, M., Das, S., Arias, J.C., Seppälä, J., Sun, Z., Vapaavuori, J., 2024. Light-driven multidirectional bending in artificial muscles. Adv. Mater., 2405917
Maga, D., Hiebel, M., Thonemann, N., 2019. Life cycle assessment of recycling options for polylactic acid. Resour. Conserv. Recycl. 149, 86–96. https://doi.org/10.1016/j.resconrec.2019.05.018.
Mahmud, M.A.P., Farjana, S.H., 2022. Comparative life cycle environmental impact assessment of renewable electricity generation systems: a practical approach towards Europe, North America and Oceania. Renew. Energy 193, 1106–1120. https://doi.org/10.1016/j.renene.2022.05.031.
Mardlin, K., Osazuwa, O., Kontopoulou, M., Leelapornpisit, W., 2022. Polyamide composites containing graphene nanoplatelets produced via thermomechanical exfoliation. Compos. Sci. Technol. 225, 109493. https://doi.org/10.1016/j.compscitech.2022.109493.
Matuštík, J., Hnátková, T., Kočí, V., 2020. Life cycle assessment of biochar-to-soil systems: a review. J. Clean. Prod. 259, 120998. https://doi.org/10.1016/j.jclepro.2020.120998.
Meng, F., Brandão, M., Cullen, J.M., 2024. Replacing plastics with alternatives is worse for greenhouse gas emissions in most cases. Environ. Sci. 58, 2716–2727..
Mi, J., Li, X., Niu, S., Zhou, X., Lu, Y., Yang, Y., Sun, Y., Meng, Q., 2024. High-strength and ultra-tough supramolecular polyamide spider silk fibers assembled via specific covalent and reversible hydrogen bonds. Acta Biomater. 176, 190–200. https://doi.org/10.1016/j.actbio.2024.01.004.
Mohammed, Z., Jeelani, S., Rangari, V., 2022. Effective reinforcement of engineered sustainable biochar carbon for 3D printed polypropylene biocomposites. Composites Part C: Open Access 7, 100221.
Moncada, J., Vural Gursel, I., Huijgen, W.J.J., Dijkstra, J.W., Ramírez, A., 2018. Techno-economic and ex-ante environmental assessment of C6 sugars production from spruce and corn. Comparison of organosolv and wet milling technologies. J. Clean. Prod. 170, 610–624. https://doi.org/10.1016/j.jclepro.2017.09.195.
Morão, A., De Bie, F., 2019. Life cycle impact assessment of polylactic acid (PLA) produced from sugarcane in Thailand. J. Polym. Environ. 27, 2523–2539.
Mousavi, Z., Heuzey, M.-C., Carreau, P.J., 2023. Compatibilized polylactide/polyamide 11 blends containing multiwall carbon nanotubes: morphology, rheology, electrical and mechanical properties. Polymer (Guildf) 276, 125906. https://doi.org/10.1016/j.polymer.2023.125906.
Mozrall, A.M., Hernandez-Charpak, Y.D., Trabold, T.A., Diaz, C.A., 2023. Effect of biochar content and particle size on mechanical properties of biochar-bioplastic composites. Sustain Chem Pharm 35, 101223. https://doi.org/10.1016/j.scp.2023.101223.
Nazari, A., Alimardani, M., Tavakol, M., 2024. A mechanistic approach toward understanding the mechanical and rheological properties of polyamide/reclaimed rubber blend containing silane-treated silica. Materials Today Sustainability 25, 100681. https://doi.org/10.1016/j.mtsust.2024.100681.
Nisa, Z. un, Chuan, L.K., Guan, B.H., Ahmad, F., Ayub, S., 2023. Coconut shell char-based nanocomposites of polyamide-6: an investigation of thermal, morphological, and crystalline properties. Diam. Relat. Mater. 138, 110234. https://doi.org/10.1016/j.diamond.2023.110234.
Njobet, N.L., 2012. Energy Analysis in the Extrusion of Plastics, vol. 54s. Lisans Tezi, Arcada University of Applied Science Plastics Technology Engineering, Helsinki.
Osman, A.I., Elgarahy, A.M., Mehta, N., Al-Muhtaseb, A.H., Al-Fatesh, A.S., Rooney, D. W., 2022. Facile synthesis and life cycle assessment of highly active magnetic sorbent composite derived from mixed plastic and biomass waste for water remediation. ACS Sustain Chem Eng 10, 12433–12447.
Pari, L., Suardi, A., Stefanoni, W., Latterini, F., Palmieri, N., 2020. Environmental and economic assessment of castor oil supply chain: a case study. Sustainability 12, 6339.
Peters, J.F., Iribarren, D., Dufour, J., 2015. Biomass pyrolysis for biochar or energy applications? A life cycle assessment. Environ. Sci. Technol. 49, 5195–5202.
Phiri, R., Mavinkere Rangappa, S., Siengchin, S., Oladijo, O.P., Dhakal, H.N., 2023. Development of sustainable biopolymer-based composites for lightweight applications from agricultural waste biomass: a review. Advanced Industrial and Engineering Polymer Research 6, 436–450. https://doi.org/10.1016/j.aiepr.2023.04.004.
Piccinno, F., Hischier, R., Seeger, S., Som, C., 2016. From laboratory to industrial scale: a scale-up framework for chemical processes in life cycle assessment studies. J. Clean. Prod. 135, 1085–1097. https://doi.org/10.1016/j.jclepro.2016.06.164.
Piccinno, F., Hischier, R., Seeger, S., Som, C., 2015. Life cycle assessment of a new technology to extract, functionalize and orient cellulose nanofibers from food waste. ACS Sustain Chem Eng 3, 1047–1055.
Pinto, G.M., Santos, A.B., Helal, E., Ribeiro, H., David, E., Woellner, C.F., Demarquette, N.R., Fechine, G.J.M., 2023. Exploring the relationship between interfacial adhesion, molecular dynamics, and the brill transition in fully bio-based polyamide 1010 nanocomposites reinforced by two-dimensional materials. Polymer (Guildf) 289, 126482. https://doi.org/10.1016/j.polymer.2023.126482.
Quiles-Carrillo, L., Boronat, T., Montanes, N., Balart, R., Torres-Giner, S., 2019. Injection-molded parts of fully bio-based polyamide 1010 strengthened with waste derived slate fibers pretreated with glycidyl- and amino-silane coupling agents. Polym. Test. 77, 105875. https://doi.org/10.1016/j.polymertesting.2019.04.022.
Raja, T., Devarajan, Y., 2025. Study on the mechanical and thermal properties of basalt fiber-reinforced lead oxide nanoparticle polymer composite for advanced energy storage applications. J. Energy Storage 108, 115079. https://doi.org/10.1016/j.est.2024.115079.
Raja, T., Devarajan, Y., 2024. Thermal evaluation of porcelain filler particles in basalt fibre-reinforced polymer composites for thermal applications. J. Therm. Anal. Calorim. 149, 4529–4541.
Raja, T., Devarajan, Y., Logesh, K., Rajiv, A., Jagdish Upadhye, V., Tiwari, K., 2024. An in-depth investigation into the utilization of nettle fiber-reinforced epoxy composites with embedded MgO nanoparticles. Journal of Reinforced Plastics and Composites 0, 1-12.
Rajendran, S., Palani, G., Shanmugam, V., Kanagaraj, A., Veerasimman, A., Marimuthu, U., 2024. Comparative analysis of mechanical and erosion performance of cashew and sugarcane waste based biochar-reinforced polyester composites. Clean Eng Technol 18, 100718. https://doi.org/10.1016/j.clet.2023.100718.
Recupido, F., Lama, G.C., Ammendola, M., Bossa, F.D.L., Minigher, A., Campaner, P., Morena, A.G., Tzanov, T., Ornelas, M., Barros, A., Gomes, F., Bouça, V., Malgueiro, R., Sanchez, M., Martinez, E., Sorrentino, L., Boggioni, L., Perucca, M., Anegalla, S., Marzella, R., Moimare, P., Verdolotti, L., 2023. Rigid composite bio-based polyurethane foams: from synthesis to LCA analysis. Polymer (Guildf) 267, 125674. https://doi.org/10.1016/j.polymer.2023.125674.
Ren, J., 2021. Methods in Sustainability Science: Assessment, Prioritization, Improvement, Design and Optimization. Elsevier.
Ren, Y., Ren, L., Li, J., Lv, R., Wei, L., An, D., Maqbool, M., Bai, S., Wong, C.-P., 2020. Enhanced thermal conductivity in polyamide 6 composites based on the compatibilization effect of polyether-grafted graphene. Compos. Sci. Technol. 199, 108340. https://doi.org/10.1016/j.compscitech.2020.108340.
Röder, H., Kumar, K., Füchsl, S., Sieber, V., 2022. Ex-ante life cycle assessment and scale up: a protein production case study. J. Clean. Prod. 376, 134329. https://doi.org/10.1016/j.jclepro.2022.134329.
Rong, Y., Zhao, P., Shen, T., Gao, J., Zhou, S., Huang, J., Zhao, G., Liu, Y., 2023. Mechanical and tribological properties of basalt fiber fabric reinforced polyamide 6 composite laminates with interfacial enhancement by electrostatic self-assembly of graphene oxide. J. Mater. Res. Technol. 27, 7795–7806. https://doi.org/10.1016/j.jmrt.2023.11.175.
Roy, P., Defersha, F., Rodriguez-Uribe, A., Misra, M., Mohanty, A.K., 2020. Evaluation of the life cycle of an automotive component produced from biocomposite. J. Clean. Prod. 273, 123051. https://doi.org/10.1016/j.jclepro.2020.123051.
Roy, P., Tadele, D., Defersha, F., Misra, M., Mohanty, A.K., 2019. Environmental and economic prospects of biomaterials in the automotive industry. Clean Technol. Environ. Policy 21, 1535–1548.
Roy, S., Sreenivasan, H., Sarmah, A.K., Baniasadi, H., Bordoloi, S., 2025. Recent advances for CO2 mineralization in biochar-amended cementitious composites. Resour. Conserv. Recycl. 215, 108141. https://doi.org/10.1016/j.resconrec.2025.108141.
Shahnaz, T., Hayder, G., Shah, M.A., Ramli, M.Z., Ismail, N., Hua, C.K., Zahari, N.M., Mardi, N.H., Selamat, F.E., Kabilmiharbi, N., Aziz, H.A., 2024. Graphene-based nanoarchitecture as a potent cushioning/filler in polymer composites and their applications. J. Mater. Res. Technol. 28, 2671–2698. https://doi.org/10.1016/j.jmrt.2023.12.108.
Siddique, S., Leung, P.S., Njuguna, J., 2021. Drilling oil-based mud waste as a resource for raw materials: a case study on clays reclamation and their application as fillers in polyamide 6 composites. Upstream Oil and Gas Technology 7, 100036. https://doi.org/10.1016/j.upstre.2021.100036.

Sobhan, A., Muthukumarappan, K., Wei, L., Qiao, Q., Rahman, M.T., Ghimire, N., 2021. Development and characterization of a novel activated biochar-based polymer composite for biosensors. Int. J. Polym. Anal. Char. 26, 544–560.

Tadele, D., Roy, P., Defersha, F., Misra, M., Mohanty, A.K., 2020. A comparative life-cycle assessment of talc-and biochar-reinforced composites for lightweight automotive parts. Clean Technol. Environ. Policy 22, 639–649.

Tang, Y.-L., Zheng, G.-Q., Lin, Y.-X., Lu, P., Zhao, H.-B., Guo, D.-M., Chen, L., Liu, B.-W., Wang, Y.-Z., 2023. Bio-based long-chain aliphatic polyamide with intrinsic flame retardancy and great overall properties. Polym Degrad Stab 214, 110416. https://doi.org/10.1016/j.polymdegradstab.2023.110416.

Tsalidis, G.A., Korevaar, G., 2022. Environmental assessments of scales: the effect of ex-ante and ex-post data on life cycle assessment of wood torrefaction. Resour. Conserv. Recycl. 176, 105906. https://doi.org/10.1016/j.resconrec.2021.105906.

Vidal, J.L., Yavitt, B.M., Wheeler, M.D., Kolwich, J.L., Donovan, L.N., Sit, C.S., Hatzikiriakos, S.G., Jalsa, N.K., MacQuarrie, S.L., Kerton, F.M., 2022. Biochar as a sustainable and renewable additive for the production of Poly (ε-caprolactone) composites. Sustain Chem Pharm 25, 100586.

Wan, T., Liao, S., Wang, K., Yan, P., Clifford, M., 2013. Multi-scale hybrid polyamide 6 composites reinforced with nano-scale clay and micro-scale short glass fibre. Compos Part A Appl Sci Manuf 50, 31–38.

Wang, X.-Z., He, J., Weng, Y.-X., Zeng, J.-B., Li, Y.-D., 2019. Structure-property relationship in fully biobased epoxidized soybean oil thermosets cured by dicarboxyl terminated polyamide 1010 oligomer with different carboxyl/epoxy ratios. Polym. Test. 79, 106057.

Ye, P., Guo, B., Qin, H., Wang, C., Li, J., Chen, Y., Lu, D., Wang, L., Gao, P., Ma, P., Zhan, B., Yu, Q., 2024. Investigation of the properties and sustainability of modified biochar-doped cement-based composite. Cem. Concr. Compos. 153, 105684. https://doi.org/10.1016/j.cemconcomp.2024.105684.

Ye, X., Meng, X., Han, Z., Qi, Y., Li, Z., Tian, P., Wang, W., Li, J., Li, Y., Zhang, W., Yang, R., 2023. Designing Fe-containing polyhedral oligomeric silsesquioxane to endow superior mechanical and flame-retardant performances of polyamide 1010. Compos. Sci. Technol. 233, 109894. https://doi.org/10.1016/j.compscitech.2022.109894.

Yiga, V.A., Lubwama, M., Karemani, D., Bbosa, D., Olotu, E.B.O., Olupot, P.W., Natukunda, F., 2023. Prediction of tensile strength of biochar filled polylactic acid composites via box-behnken design. Journal of Engineering Research, 100142. https://doi.org/10.1016/j.jer.2023.100142.

Zhang, Q., Chen, J., Guo, X., Lei, H., Zou, R., Huo, E., Kong, X., Liu, W., Wang, M., Ma, Z., Li, B., 2024. Mussel-inspired polydopamine-modified biochar microsphere for reinforcing polylactic acid composite films: emphasizing the achievement of excellent thermal and mechanical properties. Int. J. Biol. Macromol. 260, 129567. https://doi.org/10.1016/j.ijbiomac.2024.129567.

Zhang, Q., Wang, R., Liu, W., Yang, Y., Huang, L., Huo, E., Ma, Z., 2023. New strategy for reinforcing polylactic acid composites: towards the insight into the effect of biochar microspheres. Int. J. Biol. Macromol. 245, 125487. https://doi.org/10.1016/j.ijbiomac.2023.125487.

Zhang, Q., Zhang, D., Lu, W., Khan, M.U., Xu, H., Yi, W., Lei, H., Huo, E., Qian, M., Zhao, Y., Zou, R., 2020a. Production of high-density polyethylene biocomposites from rice husk biochar: effects of varying pyrolysis temperature. Sci. Total Environ. 738, 139910. https://doi.org/10.1016/j.scitotenv.2020.139910.

Zhang, Q., Zhang, D., Xu, H., Lu, W., Ren, X., Cai, H., Lei, H., Huo, E., Zhao, Y., Qian, M., 2020b. Biochar filled high-density polyethylene composites with excellent properties: towards maximizing the utilization of agricultural wastes. Ind. Crops Prod. 146, 112185.

Zhou, N., Xia, L., Jiang, N., Li, Y., Lyu, H., Zhang, H., Zou, X., Liu, W., Zhang, D., 2024. Enhanced interfacial bonding of AF/PEEK composite based on CNT/aramid nanofiber multiscale flexible-rigid structure. J. Mater. Sci. Technol. https://doi.org/10.1016/j.jmst.2024.02.015.

Zhu, X., Labianca, C., He, M., Luo, Z., Wu, C., You, S., Tsang, D.C.W., 2022. Life-cycle assessment of pyrolysis processes for sustainable production of biochar from agro-residues. Bioresour. Technol. 360, 127601. https://doi.org/10.1016/j.biortech.2022.127601.

Zhu, Xiefei, Zhang, Y., Ding, H., Huang, L., Zhu, Xifeng, 2018. Comprehensive study on pyrolysis and co-pyrolysis of walnut shell and bio-oil distillation residue. Energy Convers. Manag. 168, 178–187. https://doi.org/10.1016/j.enconman.2018.05.012.

Zierdt, P., Theumer, T., Kulkarni, G., Däumlich, V., Klehm, J., Hirsch, U., Weber, A., 2015. Sustainable wood-plastic composites from bio-based polyamide 11 and chemically modified beech fibers. Sustainable Materials and Technologies 6, 6–14. https://doi.org/10.1016/j.susmat.2015.10.001.

Sphera, LCA for Experts, 2024b. https://sphera.com/solutions/product-stewardship/life-cycle-assessment-software-and-data/lca-for-experts/. Accessed November 18, 2023.

Sphera, Managed LCA Content, 2024a. https://sphera.com/solutions/product-stewardship/life-cycle-assessment-software-and-data/managed-lca-content/. Accessed 18 November, 2023.